

https://dspace.org/

Characterization of a new reference class ionization chamber

Maphumulo, Nkosingiphile

2021
https://hdl.handle.net/10539/32369

Downloaded from a DSpace repository. https://dspace.org/



CHARACTERIZATION OF A NEW REFERENCE CLASS IONIZATION CHAMBER

Nkosingiphile Maphumulo

A dissertation submitted to the School of Physics, University of the Witwatersrand, Johannesburg, in partial fulfilment of the requirements for the degree of:

Master of Science in Physics

Johannesburg; 2021

Abstract

The aim of this study was to determine the clinical dosimetric performance of a new 3D ionization chamber (PTW-31021) designed for measurements in both standard and nonstandard clinical beams. Beam quality correction factors for standard beams and field output factor correction factors for nonstandard beams were derived, and recommendations were made on the smallest field for which the detector can still provide reliable results.

All measurements were performed using a Siemens Primus linear accelerator and a Theratron Equinox Cobalt-60 teletherapy unit. The long term stability of the PTW-31021 was evaluated in the Cobalt-60 beam. The effective point of measurement for the PTW-31021 was determined by comparing the relative depth ionization curve measured with the PTW-31021 set up to the reference point as defined by the manufacture, to the relative depth ionization curve measured with an Advanced Markus chamber (PTW-34045). The energy dependence of the PTW-31021 was determined by comparing the absorbed dose rate measurements in water using the PTW-31021, to absorbed dose rates measured with a Farmer ionization chamber (PTW-30013) and the PTW-34045 in photon and electron beams under similar reference conditions, respectively. The small field ionization chambers used to determine the field output factors were the PTW-31018 microlion liquid ionization chamber, PTW-60012 unshielded diode, PTW-60019 microdiamond, PTW-31016 3D pinpoint ionization chamber and PTW-31010 Semiflex ionization chamber. All measurements in water were performed using the PTW-MP3 water phantom.

The PTW-31021 long term stability was found to be within 0.3%, in agreement with manufacture specifications and international recommendations of the IEC 60730. The linearity of detector response measured over a range of monitor units was also found to be within international recommendations. The effective point of measurement was found to be displaced from the reference point suggested by the manufacture by 1.3 ± 0.1 mm upstream for the chamber mounted parallel to the beam axis and 1.4 ± 0.1 mm towards the source for the perpendicular orientation. The results of the energy dependence tests showed that the PTW-31021 is energy dependent for high energy

photons and electrons, and the use of the detector in beam qualities different from the calibration beam, will require a correction factor for energy dependence. Field output factor correction factors for the PTW-31021 were determined for field sizes: 8 x 8, 6 x 6, 4 x 4, 3 x 3, 2.5 x 2.5, 2 x 2, 1.5 x 1.5 and 1.2 x 1.2 cm^2 in accordance with the IAEA TRS-483 code of practice [22].

Keywords

PTW-31021; Semiflex 3D ionization chamber; Dosimetry; Small fields; Field output factors

Declaration

I, NKOSINGIPHILE MAPHUMULO, declare that this Dissertation is my own, unaided work. It is being submitted for the Degree of Master of Science in Physics at the University of the Witwatersrand, Johannesburg. It has not been submitted before for any degree or examination at any other University.



NKOSINGIPHILE MAPHUMULO

April 2021

Dedication

In memory of my parents

Thembelihle Charity Maphumulo and Vivian Mbhekeni Maphumulo

Acknowledgements

Acknowledgement to my supervisor, Professor Debbie van der Merwe for the support and encouragement during the project.

Charlotte Maxeke Johannesburg Academic Hospital and the University of the Witwatersrand are acknowledged for supporting this project. The research project was evaluated by the University of the Witwatersrand Human Research Ethics Committee (Medicine) and did not involve human subjects. A waiver of ethics clearance was obtained (Ref: W-CJ-151204-1).

Zakithi Msimang and Lazola Nobecu are acknowledged for their useful discussions, encouragement and assistance with some of the measurements. PTW-Freiburg is acknowledged for the loan of several detectors used in the study.

The support of close friends and family during the study is also appreciated.

Contents

Abstract **II**

Declaration **IV**

Dedication **V**

Acknowledgements **VI**

Authors Preface **IX**

Introduction . . . .…….…… ……..1

1.1 Aim . . . .……..……...3

1.2 Objective . . . .……..…….....3

Chapter 2 Scientific Background. . . . . ……. ..……..……..…4

2.1 Cavity Theory . . . .……...……..……4

2.1.1 Bragg-Gray cavity theory……...4

2.1.2 Spencer-Attix formalism……6

2.2 Detectors . . . .……..…....7

2.2.1 Air Ionization chambers……7

2.3 Dosimetry in the clinic . . . . . ……...… ……..….10

2.4 Static small field Dosimetry in high energy photon beams. ……. .. . . . . ……...14

2.4.1 Lateral Charged Particle Equilibrium ……...14

2.4.2 Partial Source Occlusion ……...17

2.4.3 Detector Specific Influence in Small Static Fields ……18

Chapter 3 Materials and Methodology . . . . . ……...……....20

3.1 Beams and detectors …….. . . . . .. ……...……...20

3.2 Semiflex 3D PTW-31021……. . . . . ……..21

3.2.1 Chamber long term stability …..……...…….……...…..22

3.2.2 Setting up the PTW MP3 water phantom……...……..23

3.2.3 Chamber response linearity…….……...……..26

3.2.4 Measurement of the effective point of measurement in Photon beams……...……...……..26

3.2.5 Pre-irradiation and post-irradiation leak current.……..……...28

3.2.6 Beam quality dependence……..……..…….……29

3.2.7 Field output correction factors in small photon fields ……..….35

Chapter 4 Results and Discussion ……...……..39

4.1 Chamber long term stability ……...……..39

4.2 Chamber response linearity ……...……...……40

4.3 Verification of the effective point of measurement ……...…….……..41

4.4 Pre-irradiation and post-irradiation leak current ……..……..…,……..45

4.5 Energy quality dependence……...……...……..45

4.6 Correction factor for field output factors in small fields ……...,……..50

Chapter 5 Conclusions……...……...……..56

Bibliography ……..……...…58

Appendix ……...……65

Manufacture Specification of PTW-31021 Semiflex 3D Ionization chamber...65

Author's Preface

This study is aimed at investigating the clinical dosimetric characteristics of a new PTW-31021 air ionization chamber. Chapter 1 provides a brief introduction to radiotherapy dosimetry. Chapter 2 provides the scientific background of the theory used to determine absorbed dose to a medium from measurements with vented air ionization chambers, design characteristics of air ionization chambers and dosimetry in clinical practice including methodologies used in small fields. Chapter 3 provides detailed specifications of the beams, detectors and other instruments used in the study such as environmental loggers and phantoms. This section also provides detailed descriptions of the methods used in performing the various tests for characterization of the ionization chamber. Chapter 4 provides the results of the tests and a discussion of the results. Results of new data on the PTW-31021 are also provided in this section, such as beam quality correction factors for standard beams and field output factor correction factors for small static fields. Chapter 5 provides concluding remarks on the results of the investigation and highlights the advantages and limitations of the PTW-31021 ionization chamber.

Chapter1 Introduction

Radiation therapy is a specialty in medicine that uses ionizing radiation for the treatment or management of cancer [6]. Radiotherapy techniques use high energy photons or charged particles to deliver tumoricidal doses to cancerous cells graphically represented as a target volume [7]. The absorbed dose to a medium is defined as the energy imparted to a known mass (m) in a medium and the effectiveness of radiotherapy treatment lies in the accuracy of absorbed dose delivery to the target volume [8]. Ionizing radiation directed to cancerous tissue destroys cancer cells by causing damage to their DNA strands and thus attaining tumour control [9]. Hence, the primary objective of a radiotherapy treatment is to obtain maximum tumour control with minimal normal tissue complications for patients receiving radical treatment and to improve the quality of life for those patients that are being treated palliatively [10]. There are numerous factors that can influence the accuracy of dose delivery to the target volume but this study will focus on dosimetry. Dosimetry in radiotherapy refers to the measurement of absorbed dose to water, which starts with the measurement of the absolute absorbed dose at a point in a medium under reference conditions. This then leads to normalized relative absorbed dose distributions in a volume for a range of conditions [11]. For accurate dose delivery and high quality treatments, treatment devices need to be properly calibrated and accurate data need to be acquired for use in treatment planning systems [12].

There is a wide range of detectors available commercially that can be used for absolute as well as relative dosimetry. Vented ionization chambers are recognized as the gold standard for commissioning and calibration of clinical high energy photon and electron beams [15]. This is because ionization chambers exhibit a linear response with absorbed dose and have relatively low dependency on beam energy, dose rate, type of radiation and field size under equilibrium conditions [16]. However, the ever-

increasing use of small, non-equilibrium radiation fields in radiotherapy has led to new dosimetric challenges not addressed by conventional dosimetry codes of practices [17]. An example of these challenges would be performing measurements in conditions where lateral charged particle equilibrium is not possible, performing absolute dosimetry in treatment units that cannot realise a 10 x 10 cm^2 reference field, volume averaging as a result of fluence perturbation as well as stem and cable irradiation effects observed with mini and micro-chambers [18]. In an attempt to address these challenges, detector manufacturers have resorted to producing small volume ionization chambers and solid-state detectors capable of acquiring measurements in small fields with better accuracy as compared to conventional ionization chambers [19]. Air ionization chambers are traditionally known to have lower sensitivity than solid-state detectors. Mini- and micro-ionization chambers have even lower sensitivity owing to their small active volume hence these chambers are more susceptible to stem and cable irradiation effects in large fields [20]. The lack of international guidance on how to perform accurate measurements in small fields make it difficult to compare measurements acquired under the same conditions with different detector types. The conventional definition of the radiation field size is also invalid for small fields in which collimators block part of the radiation source as observed from the center of the radiation field at the measurement depth [21]. The International Atomic Energy Agency (IAEA) in collaboration with the American Association of Physicists in Medicine (AAPM), published the first international Code of Practise (CoP) that addresses dosimetry measurements in small static high energy photon fields [22].

1.1 Aim

The aim of this study is to determine the dosimetric performance of a new 3D air ionization chamber designed for use in both standard and nonstandard high energy photon and electron fields.

1.2 Objective

In this study, the objectives are to investigate and compare the characteristics of a new reference class ionization chamber to those of other commercially available detectors. At the end of the study, the versatility and limitations of the ionization chamber will be determined and made available for the medical physics community. In this study, correction factors for field output factors will be determined experimentally in small fields using methods described in the IAEA TRS-483 CoP for small static photon fields [22].

Chapter 2 Scientific background

2.1 Cavity Theory

The measurement of absorbed dose in a medium requires the use of a radiation detector that will produce a signal that can be directly related to the imparted energy. Direct measurement of absorbed dose is possible using a calorimetry system for instance, that measures changes in temperature of an isolated medium of known mass. The amount of temperature change within the sensitive volume of the colorimeter following irradiation is then directly related to the amount of energy imparted into the medium [23]. The calorimetry method of determining absorbed dose to a medium has been used exclusively in primary standards laboratories for the establishment of absorbed dose standards. Due to the complexity associated with the calorimetry method, it is not deemed practical for routine use in the hospital setting [24]. Common practise in hospitals for estimating the beam output of a clinical linear accelerator is through implementation of international CoPs for dosimetry [24, 25].

2.1.1 Bragg-Gray cavity theory

The calibration of clinical photon and electron beams in the hospital are based on measurements done in a medium, water or air using a calibrated radiation detector, often an air ionization chamber. Direct measurement of absorbed dose to the medium using an ionization chamber is not possible. The relationship between the response of an air ionization chamber and the absorbed dose to the medium surrounding the chamber is determined through calculational methods provided by Bragg-Gray cavity theory [26, 27]. The application of this theory requires that;

- The ionization chamber cavity should be small when compared to the range of the secondary electrons such that its presence in the medium does not induce perturbation to the electron fluence [26-29].

- The energy deposited in the cavity should only be from the electrons that are crossing the cavity. This does not allow for electrons liberated in the cavity to be stopped within the cavity, hence the energy deposited by secondary electrons liberated by photon interactions within the detector is negligible when compared to the energy deposited in the sensitive volume by secondary electrons liberated in the surrounding medium that are crossing the cavity [29].

- The cavity must be positioned at a depth in a medium where charge particle equilibrium (CPE) or transient charge particle equilibrium (TCPE) conditions exist [29].

Accordingly, the relationship between the dose to the detector cavity (D_{cav}) to that of the surrounding medium (D_{med}) at depth *z* is given by;

$$\frac{D_{med}}{D_{cav}} = \frac{\emptyset_{med,z}\left(\frac{S}{\rho}\right)_{med}}{\emptyset_{cav}\left(\frac{S}{\rho}\right)_{cav}} \tag{2.1}$$

Where

$\left(\frac{S}{\rho}\right)_{med}$ and $\left(\frac{S}{\rho}\right)_{cav}$ are the average unrestricted mass collision stopping powers for the medium and the cavity at depth z respectively, this can also be written as $\left(\frac{S}{\rho}\right)_{(med,z),cav}$ [30].

Since the chamber cavity is assumed to not perturb the electron fluence in the medium according to the theory, the electron fluence in the medium at the point of interest ($\varphi_{med,z}$) is the same as the electron fluence in the chamber cavity (φ_{cav}) and equation 2.1 can therefore be written as;

$$D_{med} = D_{cav}\left(\frac{S}{\rho}\right)_{(med,z),cav} \tag{2.2}$$

2.1.2 Spencer-Attix formalism

Bragg-Gray cavity theory makes use of the average mass stopping power ratios that are derived from the electron fluence determined theoretically using the continuous slowing down approximation (CSDA) model. This model assumes that secondary electrons (electrons liberated through photon interaction with the medium) dissipate their kinetic energy through many collisional interactions of small energy loss along the electron tracks. Hence, the electron spectrum used in Bragg-Gray cavity theory to determine average stopping power ratios does not account for delta electrons (electrons liberated from hard collisions between secondary electrons and orbital electrons of the gas molecules within the cavity). From the practical work done by Attix et al, using various plane parallel ionization chambers, it was evident that the electron spectrum at the depth of the cavity for both photon and electron beams consisted of delta electrons. They were also able to prove that the electron spectrum was dependent on the atomic number of the irradiated medium as well as the size of the air cavity [26-30].

This led to a more refined cavity theory proposed by Spencer and Attix that incorporates the stopping power ratio obtained from an electron spectrum that is inclusive of secondary electrons as well as delta electrons restricted to a cutoff energy, Δ. The cutoff energy is based on the cavity size, and is the energy of electrons with a range equal to the radius of the cavity (for ionization chambers used in radiotherapy, Δ is set to be $10keV$). All delta electrons with kinetic energy less then Δ are said to deposit their energy within the sensitive volume (locally) and all electrons with energies greater then Δ are assumed to escape the cavity hence are not considered to form part of the electron fluence in the cavity [30–33].

From the Spencer Attix cavity theory, the dose to the medium is related to that of the cavity by the expression;

$$D_m = D_{cav} . S^{SA}_{med,cav} \tag{2.3}$$

where

$S_{med,cav}^{SA}$ (also written as L_{Δ}) is the Spencer-Attix average restricted mass collision stopping power ratio of the medium to the cavity [30].

The final refinement of the cavity theory was done by Nahum using Monte Carlo simulations to evaluate water to air stopping power ratios for high energy photon and electron beams [32]. Contributions by Nahum extended the Spencer-Attix theory to account for the energy deposited in the chamber cavity due to photon interactions within the air cavity [32]. The effect of considering the energy deposited in the cavity volume by electrons of energies less than Δ, i.e. dissipation by track-ends, was also evaluated. The contribution from track ends was more evident in high energy electron beams than it was in photon beams [32, 33].

2.2 Detectors

2.2.1 Air Ionization Chambers

A radiation detector is a device that produces a measurable response when exposed to radiation and this measured response can be used to determine or calculate absorbed dose in a medium [34]. The air ionization chamber is regarded as the mainstay of clinical dosimetry because of the stability and robustness in absorbed dose determination [35, 36]. An ionization chamber is characterized by a small cavity (often filled with dry air) constituting the sensitive volume, a central and an outer electrode (The central electrode is often made of a thin aluminium wire and the outer electrode is made of a thin coaxial wire mesh or thin conductive coating on the inner wall of the cavity. The chamber wall material combined with the central electrode material ought to produce an overall air equivalent device.), a chamber wall made of low Z material and a waterproofing sleeve to make the chamber water sealed as illustrated in figure 2.1 [37].

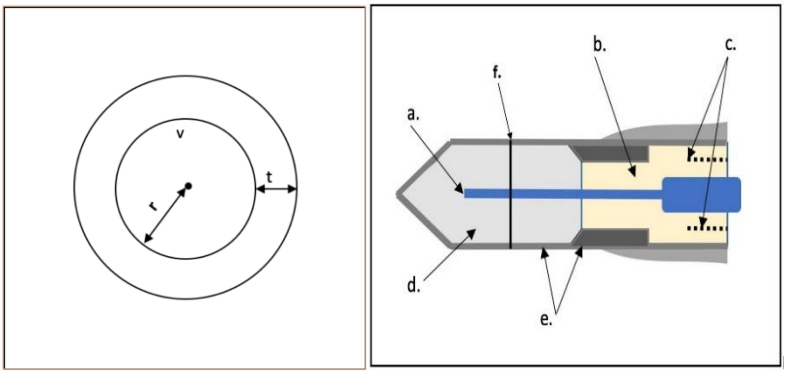

(b)

Figure 2.1: (**a**) Shows a cross sectional area schematic diagram of a Farmer type ionization chamber with a sensitive volume (v) of radius (r) filled with dry air and a wall thickness (t) and the chamber wall is made of an air equivalent material. (**b**) Shows the same chamber in the sagittal plane where (a.) central electrode, (b.) insulator, (c.) guard ring, (d.) sensitive volume, (e.) outer electrode and (f.) is the section corresponding to figure 2.1(a).

For a detector with a wall thickness much smaller than the range of the secondary electrons, such as in high-energy photon beams and standard field sizes, the cavity of a Farmer type ionization chamber behaves like a Bragg-Gray cavity [10]. The size of the sensitive volume is considered small enough not to perturb the electron fluence at the depth of measurement. However, perturbations are introduced by the difference in density between the chamber wall and the phantom medium, the central electrode and the displacement of the phantom medium by the presence of the ionization chamber. The absorbed dose to the medium (liquid water is the recommended medium for calibration of clinical beams (24, 25]) is determined using Spencer-Attix cavity theory. Determining the absorbed dose to air inside the detector requires knowledge of the total charge (C) of one sign, created in the chamber sensitive volume, the mass of air in the cavity as well as the average energy required to create an ion-pair [39]. This can be expressed as;

$$D_{air} = \frac{C}{m}\left(\frac{W_{air}}{e}\right) \tag{2.4}$$

where

C is the charge of one sign created in the chamber sensitive volume, m is the mass of air in sensitive volume and $\left(\frac{W_{air}}{e}\right)$ is the average energy required to create an ion-pair in air.

For dry air $\left(\frac{W_{air}}{e}\right) = 33.97eV$ under standard temperature and pressure as per the ICRU report 90 [40].

The absorbed dose to the medium surrounding the ionization chamber is then calculated using the Spencer-Attix cavity theory and is given by;

$$D_{m,Q} = D_{det}\left[\left(\frac{L}{\rho}\right)_{(med,z),air}\right]_{\Delta\,=\,10keV} P_Q \tag{2.5}$$

$$= \frac{C}{m}\left(\frac{W_{air}}{e}\right)\left[\left(\frac{L}{\rho}\right)_{(med,z),air}\right]_{\Delta=10keV} P_Q \tag{2.6}$$

where

$D_{m,Q}$ is the absorbed dose to the medium (m) irradiated by a beam of beam quality (Q), $\left[\left(\frac{L}{\rho}\right)_{(med,z),air}\right]_{\Delta=10keV}$ is the average restricted mass collision stopping power ratio of medium to air at depth z, and P_Q is the overall, in phantom perturbation correction factor [41].

The overall perturbation correction factor corrects for the difference between the design of the ionization chamber and an ideal Bragg-Gray cavity. For measurements in water, the overall perturbation correction factor includes correction for the non-water equivalence of the ionization chamber wall (P_{wall}), correction for water displacement by the ionization chamber cavity (P_{dis}) when the point of measurement is assumed to be in the center of the chamber sensitive volume, correction of the non-air equivalence of the central electrode (P_{cel}) and the correction for the difference in electron fluence between the air cavity and the water medium (P_{cav}). The overall perturbation factor is thus given by:

$$P_Q = P_{wall}\, P_{dis}\, P_{cel}\, P_{cav} \tag{2.7}$$

The method used to estimate the overall perturbation correction factor for a specific detector involves estimating the individual components in various steps using Monte Carlo simulations as illustrated in figure 3.4. The perturbation factors are given by the ratio of absorbed dose scored in different simulated geometries [42].

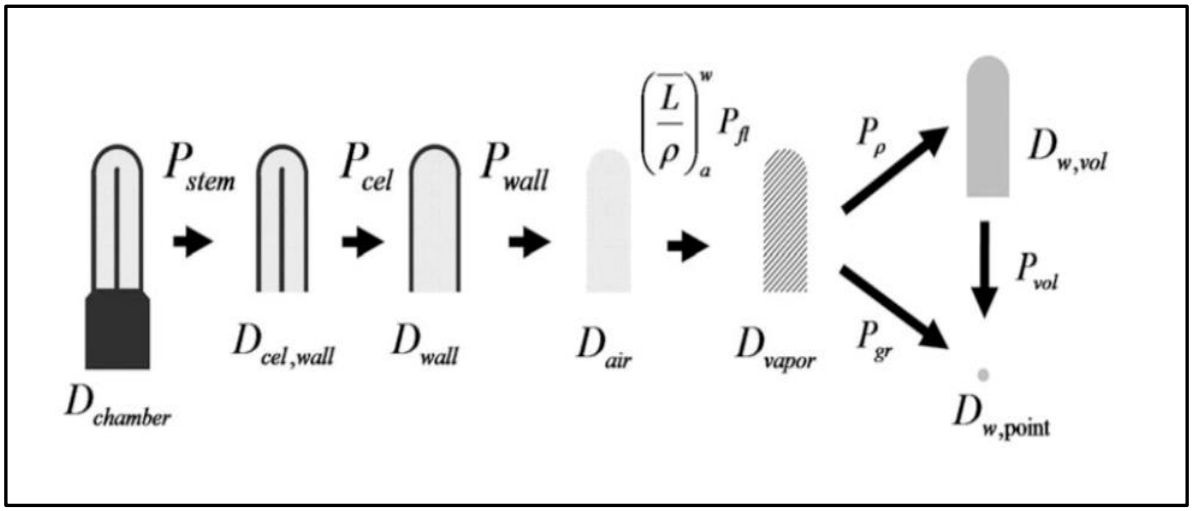

Figure 3.4: A schematic illustration of the process used to determine the series of perturbation correction factors for a specific ionization chamber using Monte Carlo. (From Bouchard et al. (2009) [42] Copyright John Wiley and Sons Inc, Reproduced with permission)

2.3 Dosimetry in the clinic

Absolute dosimetry in the hospital involves determining the absorbed dose at a specified point in water under reference conditions, using a calibrated small volume ionization chamber and this is commonly referred to as beam calibration. This is generally achieved by performing measurements in water using an air ionization chamber with an absorbed dose to water calibration factor for the particular beam quality that is traceable to Primary Standards laboratory. Uniformity and consistency in reference dosimetry practices across different hospitals in different parts of the

world is achieved through the implementation of dosimetry CoPs from international organizations, which are regarded as international standards for performing such measurements [22, 24, 25].

These CoPs include formalisms, procedures and correction factors, and specify reference conditions for converting the ionization chamber response to absorbed dose. The correction factors correct for changes in the ionization chamber response between ideal conditions and non-ideal conditions [22, 24, 25].

In 1976, in Report 24 of the International Commission on Radiation Units and Measurements (ICRU) Report on "Determination of Absorbed Dose in a Patient Irradiated by Beams of X or Gamma Rays in Radiotherapy Procedures" stated that even though not enough evidence was available at the time, an accuracy of ±5 percent in the absorbed dose to the target was necessary to eradicate the primary tumor. This uncertainty was estimated to two standard deviations that translates to a limit of 2.5 percent for combined uncertainty when reported to one standard deviation [43].

This has led to vast improvements over the years in the methods proposed in dosimetry CoPs and dosimetry protocols used internationally, with the aim of reducing the uncertainty in absorbed dose realized in the clinic.

Improvement in the accuracy to which absorbed dose to water can be estimated in the hospital was achieved with the development of calibration standards based on absorbed dose to water at Primary Standard laboratories [46]. The most commonly used dosimetry protocols and CoPs today rely on the use of an ionization chamber calibrated in terms of absorbed dose to water in a Cobalt-60 beam under reference conditions [24, 25].

In accordance with recommendations in the dosimetry CoP TRS-398 of the IAEA, the formalism to estimate absorbed dose to water at reference depth ($D_{w,z_{ref},Q}$) in high energy photon beams under reference conditions (as defined in the CoPs) is given by:

$$D_{w,z_{ref},Q} = M_{corr} N_{D,w,Q_0} k_{Q,Q_0} \tag{2.8}$$

where

M is the charge measurement at reference depth, under reference conditions and corrected for cavity-gas density variation due to differences between prevailing environmental conditions and standard environmental conditions of 20 ^{0}C and 101.35 kPa, ion collection inefficiency, polarity effects and electrometer influence for ionization chambers calibrated separate from the electrometer. N_{D,w,Q_0} is the absorbed dose to water calibration factor for the ionization chamber obtained in a Cobalt-60 beam under reference conditions as defined in the CoPs and the calibration factor is traceable to an absorbed dose to water standard that is realized and maintained at the Primary Standards laboratory [24, 25]. k_{Q,Q_0} is a factor unique to the chamber design that corrects for the difference in the chamber response due to the difference in particle energy fluence between the user's beam and the reference beam at the point of measurement also known as the beam quality correction factor [42].

The beam quality correction factors for a list of commonly used ionization chambers have been provided in the protocol. They are selected based on the chamber type and beam quality of the user. The protocol defines beam quality for high energy photon beams in conventional linacs using $TPR_{20,10}$ which is the ratio of absolute dose measurements performed at a depth of 20 cm and 10 cm along the beam central axis for a fixed source to axis distance (SAD) of 100 cm and a fixed field size of 10 x 10 cm^2 defined at the isocentric plane [25]. $TPR_{20,10}$ can be very closely approximated by the ratio of charge readings corrected for influence quantities, due the insignificant variation of Spencer-Attix restricted mass stopping power ratios for water to air for Δ = 10 keV with depth as pointed out by Andreo and Nahum [47].

For electron beams, the protocol defines beam quality in conventional linacs using R_{50} which is the depth in water at which the absorbed dose to water reduces to 50 percent of its maximum value. The electron beam quality is measured using a 10 x 10 cm^2 applicator, a fixed source to surface distance (SSD) of 100 cm and an ionization chamber set up to its effective point of measurements on the beam central axis. Plane parallel ionization chambers are recommended for measurements in electron beams and the protocol does not advise the use of cylindrical ionization chambers in electron

beams with mean electron energies of less than 10 MeV. Measurements acquired using ionization chambers yields relative ionization curves from which $R_{50,ion}$ is determined, $R_{50,ion}$ is the depth in water in which the ionization chamber response, reduces to 50 percent of its maximum value. The protocol provides a formalism to convert $R_{50,ion}$ to R_{50} [25].

For detectors produced after the publication of the IAEA TRS-398 CoP and not included in the list of detectors with their beam quality correction factors, formalisms have been provided in the code for estimating these factors [25].

There are two Monte Carlo methods recommended for determining the beam quality correction factors k_{Q,Q_0} for an ionization chamber. One involves determining the values of the overall perturbation correction factors in the reference beam and the user beam as illustrated in figure 3.4 above and then applying equation 2.9 given by [47].

$$k_{Q,Q_0} = \frac{\left(S_{w,air}\right)_Q}{\left(S_{w,air}\right)_{Q_0}} . \frac{P_Q}{P_{Q_0}}$$

$$= \frac{\left[P_{wall}\, P_{repl} \left(\frac{\bar{L}}{\rho}\right)_{air}^{water}\right]_Q}{\left[P_{wall}\, P_{repl} \left(\frac{\bar{L}}{\rho}\right)_{air}^{water}\right]_{Q_0}} \tag{2.9}$$

$$P_Q = [P_{cav}.P_{dis}.P_{wall}.P_{cel}] \tag{2.10}$$

where

P_Q and P_{Q_0} are total perturbation correction factors in the user beam and the calibration beam respectively. In equation 3.10, P_{cav} corrects for the influence of the chamber cavity, P_{dis} corrects for the displacement of the water by the chamber, P_{wall} corrects for the difference in density between the chamber wall

and the water medium and P_{cel} corrects for the effects of the central electrode. $(S_{w,air})_Q$ are restricted mass stopping power ratios for water and air that are available in literature for common beam energies.

The second method involves simulating the absorbed dose in water in the absence of the ionization chamber and in the chamber cavity for both the user beam and the Cobalt-60 beam. This method follows the assumption that the average energy expanded to create an ion pair in air is constant for Cobalt-60 and the user's beam. The beam quality correction factor is then calculated from the expression;

$$k_{Q,Q_0} = \frac{\left(\frac{D_w}{D_{ch}}\right)_Q}{\left(\frac{D_w}{D_{ch}}\right)_{Q_o}} \tag{2.11}$$

where

D_w is the simulated absorbed dose in water and D_{ch} is the absorbed dose in the chamber cavity [48-50].

The advantage of the two Monte Carlo methods, is that they provide data in situations for which measurement are not possible. The first Monte Carlo method is superior to the later because it estimates individual perturbation correction factors that are then used to determine the combined perturbation correction factor however, this is also more taxing in the number of simulations required as well as time required to set-up the Monte Carlo code [50].

2.4 Static small field dosimetry in high energy photon beams

Small field dosimetry refers to the practice of dosimetry in conditions where the radiation field size makes it challenging to accurately estimate dose due to the finite dimensions of radiation detectors as pointed out by Das et al. [54].

The currently accepted definition of a small field is defined as any radiation beam that satisfies at least one of the following three conditions;

- There is lack of lateral charged particle equilibrium (LCPE) at a point in the beam central axis and reference depth.
- There is partial source occlusion by the collimation system as observed from the beam central axis at the measurement depth.
- The detector lateral diminutions (detector size) are similar or large compared to the radiation field size at the measurement depth [48, 56].

2.4.1. Lateral Charged particle equilibrium

Loss of LCPE is defined as a condition determined in the center of the radiation beam at reference depth in which the half width or radius of the radiation field is smaller than the maximum range of the majority of the secondary electrons [55]. The minimum radius of a radiation field in which lateral charged particle equilibrium exists was first quantified by Li at al. [57] in which, using Monte Carlo simulations, the ratio of absorbed dose to water against collision kerma for various circular fields of radius below 3 cm, were calculated. The calculations were done in the center of the field at a depth of 5 cm and normalized to 10 x 10 cm^2 for photon beams of various beam quality. Figure 2.4 shows the results of the ratio of absorbed dose to collision kerma in the ionization chamber cavity for multiple beams of various beam qualities as a function of radiation field radius acquired from Monte Carlo simulations. The lateral charged particle equilibrium radius (r_{LEE}) was defined as the field radius in which the ratio of absorbed dose to collision kerma in the chamber cavity becomes lower than that determined for conventional radiation fields (10 x 10 cm^2).

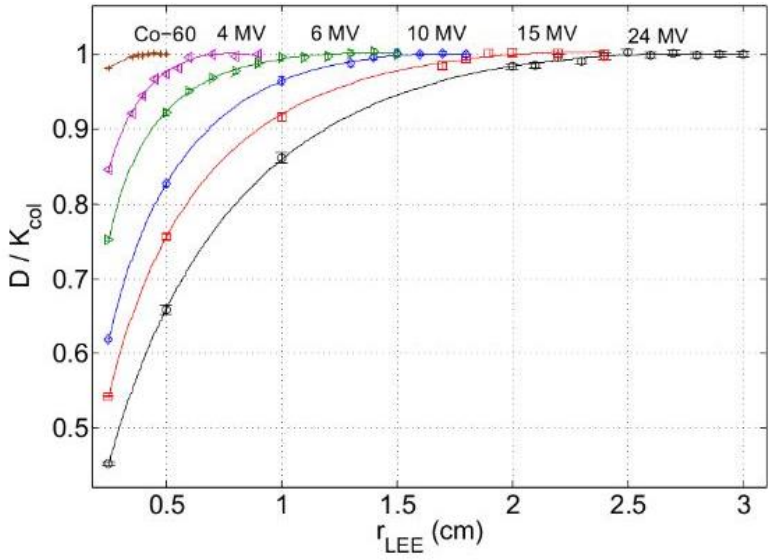

Figure 2.4: The ratio of absorbed dose to water and collision kerma calculated using Monte Carlo calculations, in the center of circular beams at a depth of 5 cm for various beam qualites. The calculations were done at 80 cm SSD for a Cobalt-60 beam and at 100 cm SSD for the higher energy photon beams. The data was normalized to the ratio of absorbed dose to water/ collision kerma calculated in a 10 x 10 cm^2 broad beam for the same 5cm depth [58]. (From Pavlos Papaconstadopoulos, On the detector response and the reconstruction of the source intensity distribution in small photon fields, PhD thesis, McGill University, Montréal. © 2016. Reproduced with permission)

The IAEA TRS-483 CoP provides a formalism to calculate the LCPE range as a function of beam quality index, which is given by:

$$r_{LCPE} = 8.369\,.TPR_{20,10}(10) - 4.382 \tag{2.14}$$

$$r_{LCPE} = 77.97 \times 10^{-3}\,.\%dd(10,10)_X - 4.112 \tag{2.15}$$

where

r_{LCPE} is the LCPE range, $TPR_{20,10}(10)$ is the beam quality index defined as the tissue phantom ratio measured at depth 20 cm and 10 cm for a 10 x 10 cm^2 square field and $\%dd(10,10)_X$ is the beam quality index defined as X-rays only percent depth dose measured at a depth 10 cm from the water surface for a 10 x 10 cm^2 square field.

CoPs recommend that absolute dosimetry should be performed in a reference field of 10 x 10 cm^2 [24, 25]. For treatment units that cannot realize a 10 x 10 cm^2 reference field, the IAEA TRS-483 CoP recommends the concept of a machine specific reference (msr) field and a formalism to estimate beam qualities for a 10 x 10 cm^2 based on measurements performed in the msr field [22].

For machines that can realise the reference field size of 10 x 10 cm^2, it is recommended in IAEA TRS-483 that reference dosimetry be performed following conventional methods. For machines that cannot realise the reference field proposed in conventional CoPs, reference dosimetry should be done in the msr field. It is recommended that the msr field and detector combination satisfy the condition:

$$FWHM \geq 2 * r_{LCPE} + d \tag{2.16}$$

where

FWHM is the measured radiation field size, r_{LCPE} is the lateral charged particle equilibrium range in g/cm^2 and d is the diameter of a cylindrical detector measured from the outer surface of the detector.

2.4.2. Partial source Occlusion

Partial source occlusion occurs when the physical field size is the same or smaller than the source spot size as viewed from the beam central axis at the measurement depth [59]. This phenomenon results in reduced beam output and overlapping penumbra that leads to the radiation field size defined by the FWHM, becoming significantly larger than the geometrical field size as pointed out by Das et al. [60]. Hence the protocol recommends defining the field size using the irradiation field (FWHM) and not the geometrical set field defined by the collimation system.

Figure 2.6 illustrates the effect of partial source occlusion on the radiation fields size relative to the geometrical field size and shows that in small fields, the congruency between the radiation field and the geometrical field does not exist.

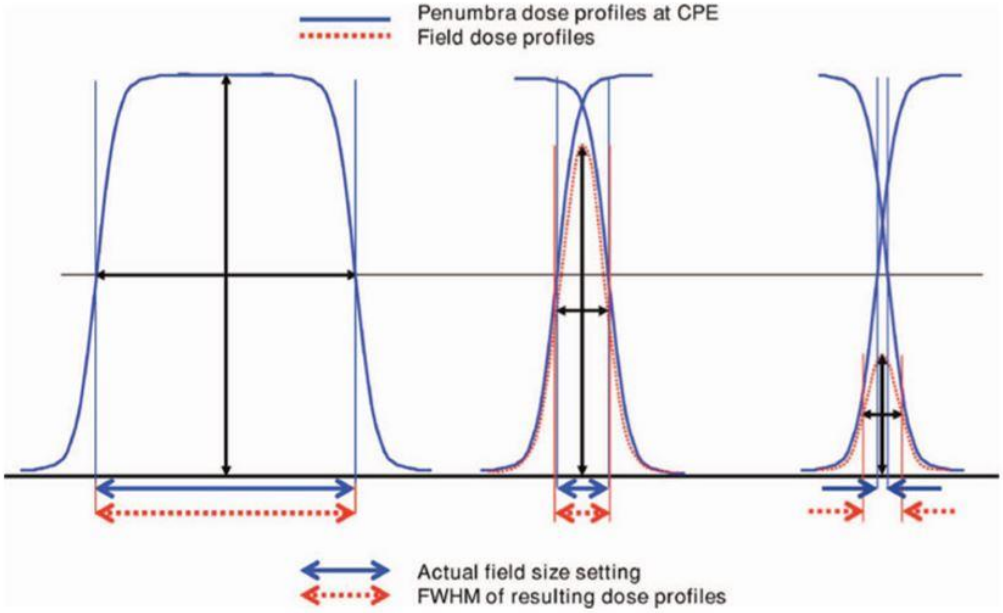

Figure 2.6; An illustration the effect of overlapping penumbra on the measured field size defined by the full width at half maximum (FWHM) as observed from the measurement depth. On the far left is a conventional field where the geometrical field coincides with the radiation field measured from the lateral beam profile. On the far right is an extreme case of overlapping penumbra in small fields as a result of source occlusion and lack of lateral charged particle equilibrium leading to reduced beam output and a wider field size defined by FWHM. (From Das et al. (2008) [60] Copyright John Wiley and Sons Inc, Reproduced with permission)

2.4.3. Detector specific influence in small static fields

The detector size also affects measurements in small fields, due to the perturbation of the electron fluence at the point of measurement because of the non-water equivalence of the detector [55]. The finite dimensions of the detector sensitive volume also affect measurement in small fields because it is assumed that the detector produces a signal that is averaged over the entire sensitive volume (known as volume averaging). This results in large variations between the chamber response and the actual beam profile when there are significant dose gradients [64]. Various methods have been proposed

to correct for volume averaging: one method requires the use of detectors with very good spatial resolution such as film as proposed by Casar et al. [56], and other methods involve the use of convolution kernels to obtain the true beam profile from the average absorbed dose response of the detector as demonstrated by Wegener and Sauer [67].

For measurements of field output factors, the variation in water to air stopping –power ratio for photon beams with field size is negligible [68]. Hence, the factors that influence measurements in small fields are mostly related to perturbations introduced by the presence of the chamber in the beam. For this reason, the protocol proposes a formalism for measurements of field output factors that takes care of the perturbations introduced by the detector in small fields. The formalism initially proposed by Alfonso et al [69] is given by;

$$\Omega_{Q_{clin}Q_{msr}}^{f_{clin},f_{msr}} = \frac{M_{Q_{clin}}^{f_{clin}}}{M_{Q_{clin}}^{f_{msr}}} \mathrm{k}_{Q_{clin}Q_{msr}}^{f_{clin},f_{msr}} \tag{2.17}$$

where

$\Omega_{Q_{clin}Q_{msr}}^{f_{clin},f_{msr}}$ is the field output factor measured in small fields, $M_{Q_{clin}}^{f_{clin}}$ in the detector response measured in the clinical field size (small field) and $M_{Q_{clin}}^{f_{msr}}$ is the detector response measured in the msr field.

For machines that can realize a 10 x 10 cm^2 the msr field would be a 10 x 10 cm^2 and for machines that cannot realize the reference field, the msr field would be the largest field size possible. $\mathrm{k}_{Q_{clin}Q_{msr}}^{f_{clin},f_{msr}}$ is the field output factor correction factor in small fields that corrects for the influence of the detector on the measurements. In standard fields, where $\mathrm{k}_{Q_{clin}Q_{ref}}^{f_{clin},f_{ref}}$ is unity [14].

The IAEA TRS-483 has provided tables with field output factor correction factors for a variety of detectors recommended for use in small fields [22].

Chapter 3 Materials and Methodology

3.1 Beams and detectors

An 80 cm source-axis distance Theratron Equinox Cobalt-60 teletherapy unit equipped with four independent jaws capable of realizing square/rectangular fields from 1 x 1 cm^2 up to 35 x 35 cm^2, at the isocentric plane, was used. A Siemens Primus linear accelerator having two independent jaws in the Y-axis (in-plane) and a single focused multi-leaf collimator system in the X-axis (cross-plane), was also used. All 41 leaf pairs had a projected width of 1.0 cm in the isocentric plane, and the system was capable of producing set square fields from 0.6 x 0.6 cm^2 to 40 x 40 cm^2. The single focused MLC system was capable of achieving minimum symmetric set field size of 0.6 x 0.6 cm^2. The central cross-plane major axis of the unit bisected the central leaf pair. The linear accelerator used in this study was equipped with two high energy flattened photon beams of 6 and 18 MV as well as six high energy electron beams of 6, 9, 12, 15, 18 and 21 MeV.

The detectors used were a PTW-31021 Semiflex 3D ionization chamber, PTW-31010 Semiflex ionization chamber, PTW-30013 0.6cc Farmer type ionization chamber, PTW-34045 Advanced Markus ionization chamber, PTW-31018 microlion liquid ionization chamber, PTW-60012 unshielded diode, PTW-60019 microdiamond and PTW-31016 3D pinpoint ionization chamber. The bias voltage (if relevant) was applied to the detectors using the PTW TANDEM dual channel electrometer during scanning and was substituted with a PTW Unidos E electrometer to determine integrated charge measurements for absolute dose and relative field output factor measurements. For measurements with the liquid ion chamber (PTW-31018 “microlion”), the bias voltage was applied using an external voltage supply capable of supplying bias voltage in the excess of 800 volts. The maximum achievable bias voltage with the TANDEM and Unidos E electrometers is ± 400 volts. For relative dosimetry measurement such as percent depth dose, relative ionization and lateral dose profile measurements, a PTW TBA control unit was used to control the scanning system using the PTW MEPHYSTO mc^2 version 7.42 software.

A Lufft OPUS 20 data logger was used to monitor and log the room pressure and relative humidity and a calibrated glass mercury thermometer was used to monitor the water temperature.

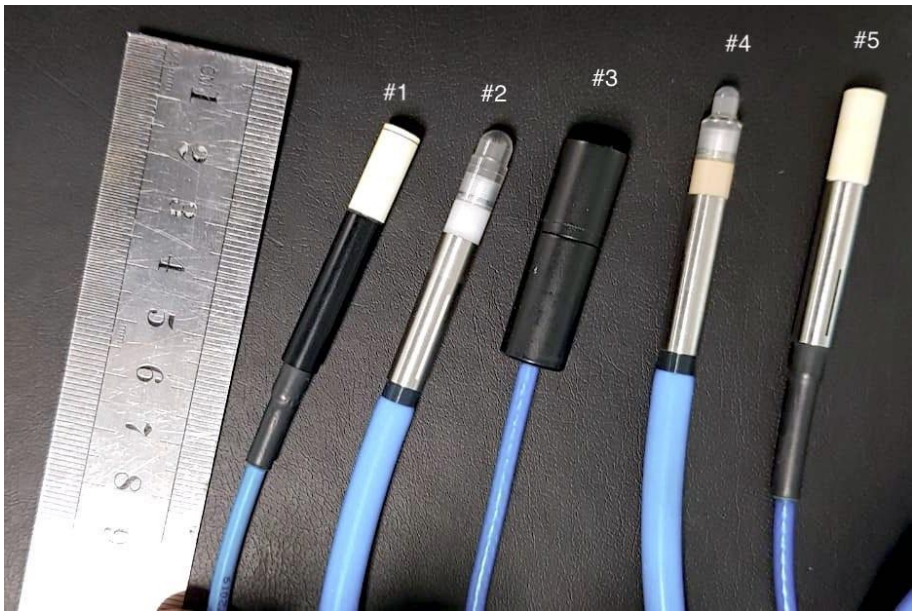

Figure 3.1: Detectors that were used for measurements in small fields. From left to right, the detectors are PTW-60019 microDiamond, PTW-31021 Semiflex 3D, PTW31018 MicroLion, PTW-31016 PinPoint 3D and PTW-60012 unshielded diode.

3.2 The Semiflex 3D PTW-31021

PTW-Freiburg introduced a new Semiflex 3D ionization chamber that was designed to be waterproof, fully guarded and capable of measurements in both standard and small fields, specified as 2.5 x 2.5 cm^2 to 40 × 40 cm^2. It has an active volume of 0.07 cm^3, a well-defined reference point (3.45 mm from chamber tip on chamber axis) and is operated at a bias voltage of 400 V. The chamber can be used in water, solid state phantoms and in air. Full specifications of this chamber can be found in the appendix section of this document.

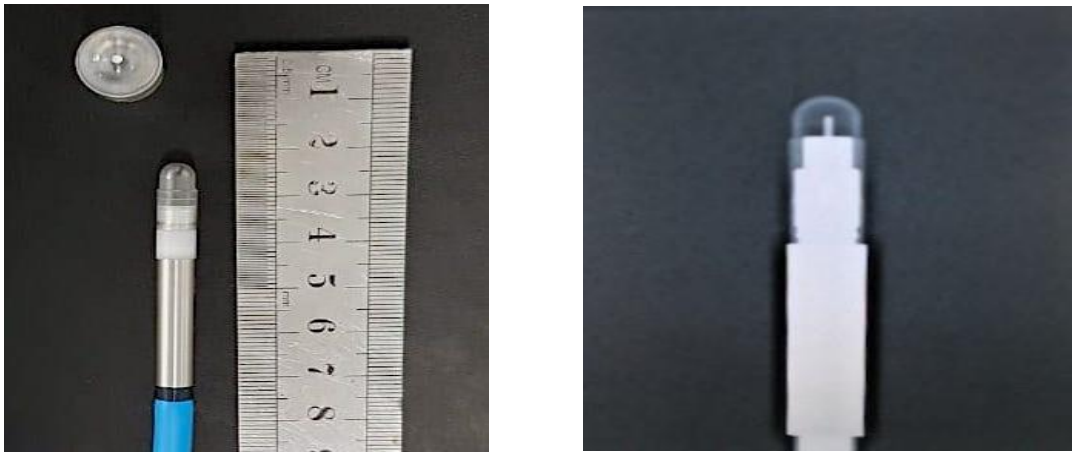

(a.) (b.)

Figure 3.2: (a) An image showing the physical appearance of the PTW-31021 Semiflex 3D ionization chamber. In the top left corner of the image is a 3mm PMMA buildup cap. (b) An X-ray radiograph of the PTW- 31021 Semiflex 3D chamber.

3.2.1 Chamber long term stability

The Semiflex 3D ionization chamber (PTW-31021) was investigated for long term stability using a Cobalt-60 teletherapy unit. Traditionally, this test is performed using a strontium-90 check source designed for the chamber However in a situation where a constancy check source is not available, a Cobalt-60 teletherapy unit (or alternative stable beam) may be used in conjunction with a highly reproducible set-up. The ionization chamber long term stability is defined as the stability of the ionization chamber response over time when exposed to the same type and radiation dose under identical exposure conditions and is often characterized by changes in the value of N_{D,W,Q_0} over time from multiple calibrations [25].

The aim of this test was to determine the stability and reproducibility of the chamber response over a relatively long period of time when exposed to the same radiation. The measurements were carried out in a perspex phantom to ensure reproducibility of the setup. The chamber was irradiated for 1 minute in the Cobalt-60 teletherapy beam in a $10 \times 10\ cm^2$ field at 80 cm from the source at a water equivalent depth of 5 g/cm^2 as illustrated in figure 3.3. For the phantom used (PMMA), the water equivalent depth was 4.4 cm. This corrects for the difference in electron fluence at the point of

measurement due to the difference in density between liquid water and PMMA phantom used [44]. The first set of measurements were used as baseline values and were compared to subsequent measurements using radioactive decay corrections.

The measurements were repeated six times over a period of 18 months and the measured charge readings were corrected for environmental conditions. The measurements were compared to the baseline value corrected for radioactive decay using the decay model defined below.

$$M_t = M_{t_0} e^{-\lambda \delta_t} \tag{3.1}$$

where

A_{t0} it the charge reading determined from the first set of measurements and corrected for influence quantities, λ is the Cobalt-60 decay constant derived its physical half-life and δt is the time difference between the first set of measurement and the current measurement.

The data were analysed by comparing the measured data and the data derived from the decay equation.

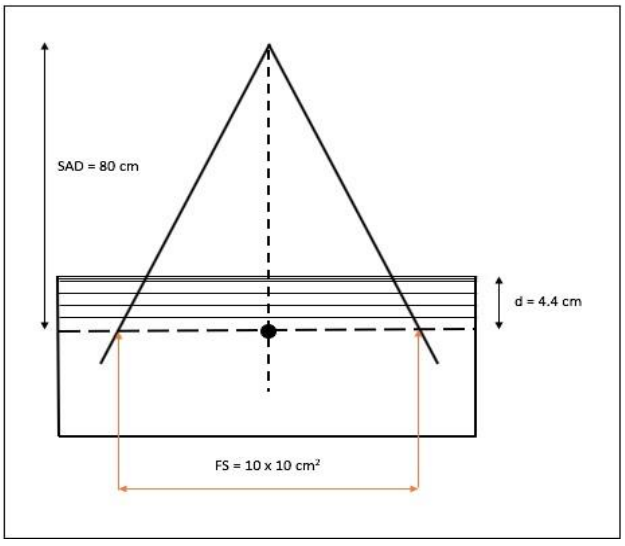

Figure 3.3: A schematic diagram of the set up used to irradiate the chamber to determine the stability of the chamber at a depth of 4.4 cm in perspex (that is equivalent to a depth of 5 cm in water). The distance from the source to the detector was 80 cm and the field size was $10 \times 10\ cm^2$.

3.2.2 Setting up the PTW MP3 water phantom

Setting up the PTW MP3 Water phantom involved positioning the phantom under the linear accelerator gantry so as to align the collimator cross wires to the markings on the phantom base, filling up the phantom with deionized water and adjusting the level of the scanning arm in the cross and in-plane direction using a spirit level placed at different positions along the scanning arm. Figure 3.4 shows a setup of a scanning water phantom positioned under the gantry with a reference detector mounted in air and a measurement detector mounted on the scanning arm.

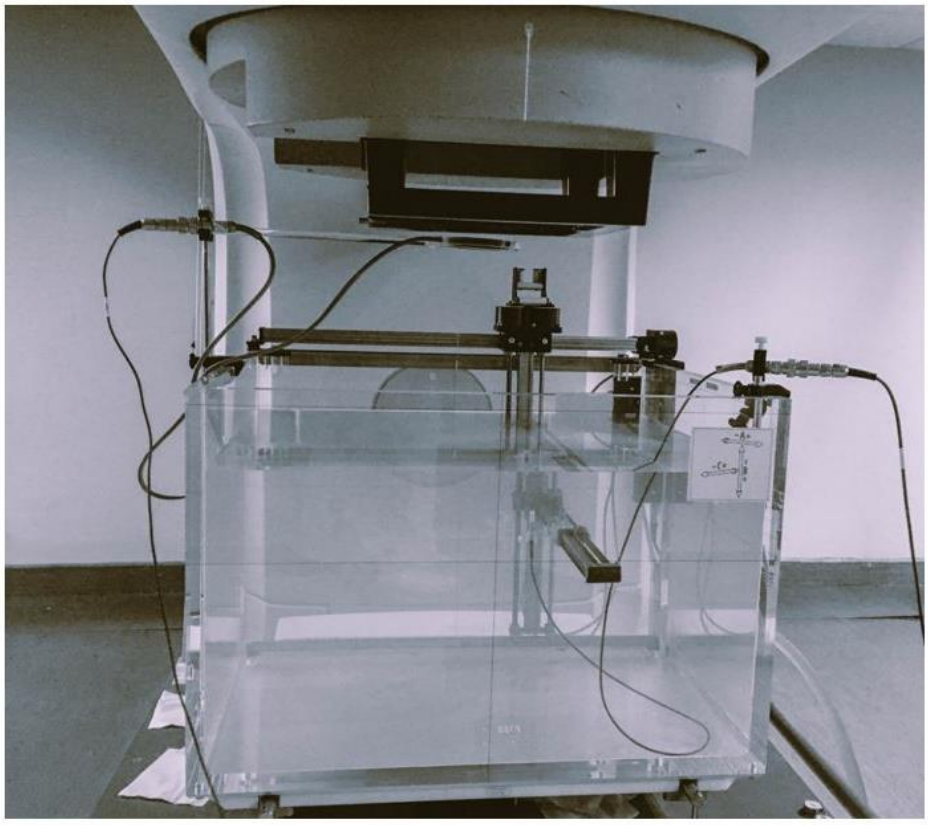

Figure 3.4: An image of the PTW MP3 scanning water phantom positioned under the gantry. In this setup a PTW-34091 T-ref chamber is positioned close to the source as a reference detector for the measurements.

An ionization chamber was then mounted onto the arm using the PTW TRUFIX ionization chamber holder and the effective point of measurement (as specified by the manufacturer) was positioned at the centre of the projected field on the surface of the water. The center of the radiation field was assumed to coincide with the cross wire projected by the light field and this was later verified through scanning. The position of the detector was set to zero thus defining the surface (depth = 0 cm). The gantry angle at 0^0 was verified using a spirit level. The source to surface distance (SSD) was set to 90 cm using the optical distance indicator (ODI). The detector was connected to the PTW TANDEM dual channel electrometer and the bias voltage was set to +400V for cylindrical ionization chambers, 300V for plane parallel ionization chambers and 0V for the solid state detectors. The PTW TANDEM dual channel electrometer was connected to the control unit that enabled remote control of the detector position and movements. To ensure that the central axis of the radiation field was exactly perpendicular to the scanning arm in the cross plane direction, the system was programmed to acquire cross-plane profiles at three different depths in the water phantom. The micro diamond detector and a field width of 4 x 4 cm^2 were used. The central axis deviation (CAX) for the beam profiles measured at the three different depths were evaluated. A perpendicular central beam axis to the phantom scanning arm was characterized by measuring the same CAX at the various depths. When the beam was found not to be perpendicular to the phantom scanning arm in the cross-pane, the results showed a systematic variation in the measured CAX values for the three depths suggesting a shift in the beam center in one direction. The tilt angle of the beam central axis was calculated as illustrated in figure 3.6 using the cross-plane lateral beam profile. The correction was applied by offsetting the gantry angle.

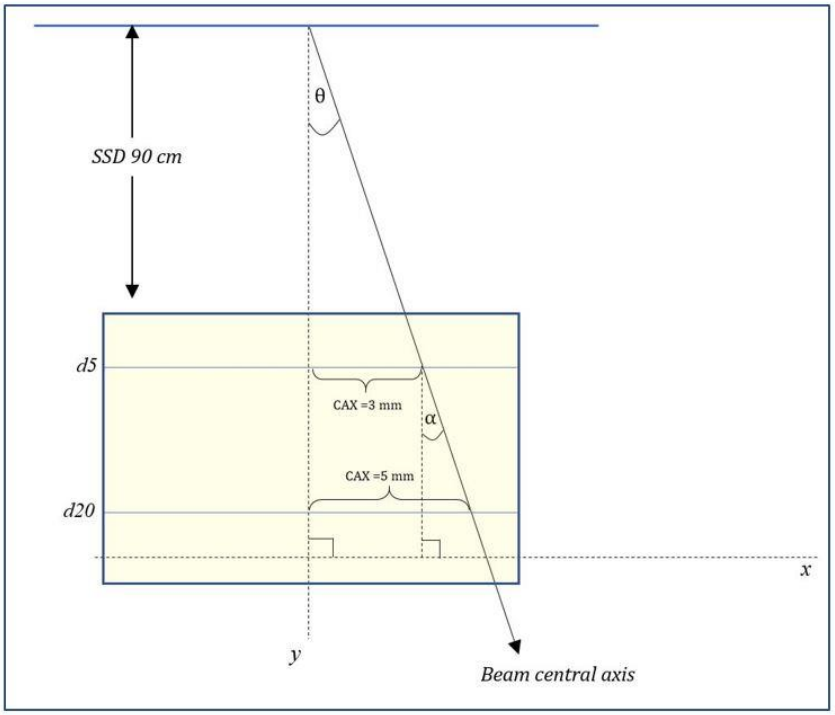

Figure 3.6: A schematic illustration of the method used to calculate the beam tilt given by the angle θ. d5 and d20 are the scanning depth of 5 cm and 20 cm respectively. The values for CAX at depth 5 and 20 cm are arbitrary values for illustration purposes.

3.2.3 Chamber response linearity

Chamber response linearity refers to the ability of the ionization chamber to produce a linear response relative to delivered dose [65]. The response linearity of the PTW-31021 was investigated in 6 and 18 MV photon beams. All measurements were performed at a depth of 10 cm from the water surface, the set field size was 10 × 10 cm^2 and a constant source to chamber distance of 100 cm was used. The chamber was irradiated with monitor units ranging from 10 MU to 640 MU and the measured charge readings were corrected for variation in temperature and pressure during the measurement sequence.

The data were analysed by plotting the measured corrected charge readings as a function of delivered monitor units and the linear coefficient was defined as the ratio of the detector response to delivered monitor units.

3.2.4 Measurement of the effective point of measurement in Photon beams

The chamber's effective point of measurement (EPOM) was determined experimentally using a plane parallel ionization chamber as the reference. The relative depth ionization curves measured using the PTW-31021 were compared with that of PTW-34045 Advanced Markus and the shift of the reference point was determined by shifting the PTW-31021 relative depth ionization curve to match that of the reference. PTW-34045 was used as the reference chamber owing to its characteristically well-defined effective point of measurement.

The measurements were performed in 6 and 18 MV photon beams using the PTW MP3 scanning system and a PTW TRUFIX chamber mount system. The first set of measurements were performed with the plane parallel chamber. The PTW-34045 was mounted on the water phantom using its dedicated holder and positioned in the centre of the field. The reference point as defined by the manufacture is located in the inner surface of the entrance window of the PTW-34045. The reference point was positioned in the surface of the water by submerging the chamber in the water, and then raising it to the water surface. The chamber was again raised by 0.9 mm, which is the distance between the surface of the waterproofing cap and the entrance window (polyethylene foil). Beam profile measurements were performed in the X and Y direction using 6 MV at 10 cm depth from the water surface for a 10×10 cm^2 field and the central axis deviation (CAX) data were used to reposition the chamber on the beam central axis. Relative depth ionization measurements were then performed along the beam central axis for a 10×10 cm^2 field size and a constant SSD of 100 cm.

The plane parallel chamber was then replaced with the PTW-31021 that was initially mounted parallel to the beams central axis. The PTW-31021 was setup using the chamber design diagrams such that the recommended reference point was positioned in the centre of the radiation field at the water surface. The centre of the radiation field was determined from lateral profiles scans measured at 10 cm depth from the water surface. Relative depth ionization measurements were performed and the results were recorded. The chamber was then mounted using a different holder such that it was perpendicular to the beam central axis. The reference point was positioned on the water

surface and centered using the CAX measurements obtained from the beam profiles. A scan of the relative depth ionization curve was performed.

In analysing the data, the relative depth ionization curves acquired using the PTW-31021 in both orientations were displaced to match the curves acquired with the PTW-34045 for 6 and 18 MV beams. The amount of displacement measured was used to define the EPOM. For the orientation in which the chamber was mounted parallel to the beam central axis, the EPOM was defined relative to the tip of the chamber and for the perpendicular orientation, it was defined relative to the chamber center. Following the shift applied to the relative depth ionization curves data acquired with the PTW-31021, the agreement between the PTW-34045 data and the PTW-31021 data were further confirmed using a gamma analysis tool.

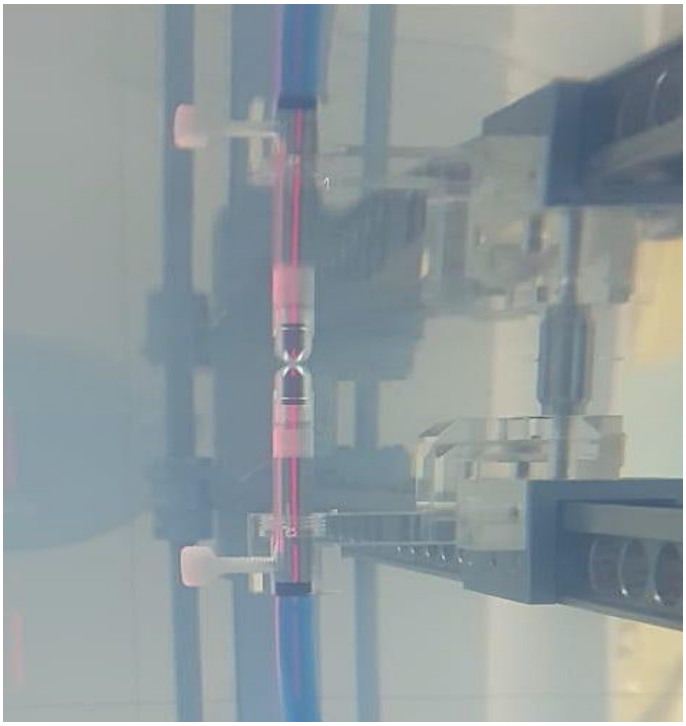

Figure 3.6: This image was taken from the side of the water phantom just below the water surface to show the Semiflex 3D ionization chamber mounted parallel to the central axis in a PTW- MP3 water phantom using a TRUFIX holder. The chamber was positioned such that it is just breaking the water surface, as represented by point in which the chamber visually coincides with its reflection when viewed from below.

3.2.5 Pre-irradiation and post-irradiation leak current

The PTW-31021 was investigated for leakage current before and after irradiation. This test was performed both in small and standard fields using 6 and 18 MV photon beams, a PTW-MP3 water phantom and a PTW Unidos E electrometer.

The chamber's effective point of measurement was positioned at the center of the radiation field at a depth of 10 cm from the water surface, the source to water surface distance was set to 90 cm and the chamber was connected to the electrometer. Three sets of measurements were performed for various field sizes covering both standard and non-standard fields. The first set of measurements were performed in the following sequence; three measurements with the beam off, three measurements with the beam on for 800 MU and the last set with the beam off immediately after the second set. All measurements were performed for 60 seconds using the electrometer internal timer. The sensitivity of the electrometer was varied between low and high range depending on the measurement performed (low range for beam off measurement and high range for beam on).

The pre-irradiation and post-irradiation leakage current was then calculated for each field size by comparing the electric charge collected pre and post irradiation, to the charge collected during irradiation.

3.2.6 Beam quality dependence

Standard photon beams

The beam quality dependence of PTW-31021 in high energy photon beams was investigated by comparing the absorbed dose to water measurements obtained with the PTW-31021 (using equation 3.4) to that of other commonly used reference ionization chambers with absorbed dose to water calibration factors determined in Cobalt-60 under reference conditions and traceable to primary standards and known beam quality dependence.

The reference ionization chambers used for the test were the PTW-30013 and PTW-31010. Absorbed dose to water measurements were performed in Cobalt-60, 6 and 18 MV beams following the recommendations of the IAEA TRS-398 CoP [25].

For each chamber, the beam quality index ($TPR_{20,10}$) measurements were performed in the 6 and 18 MV beams by taking the ratio of charge readings corrected for environmental conditions at depth 20 cm and 10 cm in the beam central axis. A fixed source to chamber distance of 100 cm and a field size of 10 x 10 cm^2 defined at the isocentric plane were maintained throughout the measurements.

The absorbed dose to water at depth 10 cm from the water surface for the reference detectors was estimated using the formalism;

$$D_{w,z,Q} = M_{corr} N_{D,w,Q_0} k_{Q,Q_0} \tag{3.3}$$

where

M_{corr} is the charge reading corrected for temperature, pressure, humidity, recombination and polarity, N_{D,w,Q_0} is the ionization chamber absorbed dose to water calibration factor in a Cobalt-60 beam and k_{Q,Q_0} is the beam quality correction factor who's values are provided in the CoP for a list of detectors and various beam quality [25].

The beam quality correction factor for the reference ionization chambers were selected according to the ionization chamber used and the measured beam quality index ($TPR_{10}^{20}(10)$).

For the PTW-31021, the absorbed dose to water at the reference depth for the various beam qualities was estimated using the formalism;

$$D_{w,z,Q} = M_{corr} N_{D,w,Q_0} \tag{3.4}$$

where

M_{corr} is the charge reading from PTW-31021 corrected for temperature, pressure, humidity, recombination and polarity and N_{D,w,Q_0} is the PTW-31021 absorbed dose to water calibration factor in a Cobalt-60 beam.

The measurement conditions used with the PTW-31021 were identical to that of the reference detectors. The resulting absorbed dose to water measured with the PTW-31021 was compared to that of the reference detectors using a graph.

The energy dependent correction factors (k_{Q,Q_0}) for 6 and 18 MV photon beams were determine from the absorbed dose to water ($D_{w,z,Q}$) measurements performed under reference conditions using the PTW-30013 as described in the work of Katumba [63]. The correction factors were calculated using the expression;

$$k_{Q,Q_0} = \frac{D^{ref}_{(w,Q,z_{ref})}}{N_{D,w,Q_0} \cdot M_{corr}} \tag{3.5}$$

where

$D^{ref}_{(w,Q,z_{ref})}$ is absorbed dose to water at a reference depth ($z_{ref} = 10\ cm$) in water measured in the user beam (6 and 18 MV) using the reference detector (PTW-30013) as defined by equations 3.3, M_{corr} is the charge reading measured with the PTW-31021 corrected for all relevant influence quantities and N_{D,w,Q_0} is the absorbed dose to water calibration factor for the PTW-31021 determined in a Cobalt-60 beam under reference condition.

The calculated k_{Q,Q_0} values were then compared to manufacture published values for the investigated beam qualities.

Standard electron beams

In electron beams, the beam quality dependence of the PTW-31021 was determined by comparing absorbed dose to water measured with the PTW-31021 to that measured with PTW-34045 and PTW-31010. All detectors had Cobalt-60 absorbed dose to water calibration factors traceable to a primary standard. The comparison was performed for absorbed dose to water measurements obtained in 12, 18 and 21 MeV electron beams.

The electron beam quality index was expressed as R_{50}, defined as the depth in water along the central axis of the electron beam under reference conditions in which the absorbed dose to water is reduced to 50% its maximum value [24, 25, 27-30].

The relative ionization readings taken along the beam central axis under reference conditions using the ionization chambers, were converted to relative dose using PTW MEPHYSTO mc^2 version 7.42 software. $R_{50,ion}$ defined as the depth in water in which relative ionization measurements are reduced to 50% of the maximum were determined for the various detectors used . The electron beam quality index for the various electron beams were then calculated from $R_{50,ion}$ values using the formalism;

$$R_{50} = 1.029\, R_{50,ion} - 0.06\, g/cm^2 \quad \ldots (R_{50,ion} \leq 10\, g/cm^2) \qquad (3.6)$$

$$R_{50} = 1.059\, R_{50,ion} - 0.37\, g/cm^2 \quad \ldots (R_{50,ion} > 10\, g/cm^2) \qquad (3.7)$$

where

$R_{50,ion}$ is the depth at which the amount of relative depth ionization measured with an ionization chamber reduces to 50% of its maximum value[25].

The calculated R_{50} values were then used to determine the reference depth for the various selected electron energies using the formalism:

$$z_{ref} = 0.6 * R_{50} - 0.1\, g/cm^2 \qquad (3.8)$$

where

z_{ref} is the reference depth in units of g/cm^2 and R_{50} is the beam quality in units g/cm^2 [25].

All measurements were performed following quality assurance on the linac beam output and for the study of the energy dependence, all measurement were performed on the same day. In each measurement session, the first measurement was repeated at the end of the series to verify stability of the output.

The chambers were then set up one after another in the water phantom using their respective holders. The chambers were positioned in the center of the field using the cross wires projected by the light field (the light field was already verified to be in congruence with the radiation field during the time of setting up the water phantom). The EPOM for the PTW-31021 mounted perpendicular to the beam axis in electron beams was found to be displaced by 1.6 ±0.2 mm from the manufacture recommended refence point away from the source towards the chamber center. This point was then adopted as the new EPOM for the PTW-31021. The PTW-31010 and PTW-34045 were set up to the EPOM recommended by the manufacture.), the field size was defined on the surface of the water using a 10 x 10 cm^2 applicator and the source to water surface distance was maintained at 100 cm.

The absorbed dose to water for the PTW-34045 and PTW-31010 was determined from the measured charge readings corrected for temperature and pressure influence, recombination and polarity using the formalism:

$$D_{w,z,Q} = M_{corr} N_{D,w,Q_0} k_{Q,Q_0} \tag{3.10}$$

where

M_{corr} is the charge reading corrected for all relevant influence quantities (temperature and pressure influence, recombination and polarity) following recommendation from TRS-398 CoP [25], N_{D,w,Q_0} is the absorbed dose to water calibration factor determined in a Cobalt-60 beam under reference conditions and k_{Q,Q_0} is the beam quality correction factor, that corrects for the change in

the ionization chamber response when it used in a beam spectrum different from that of Cobalt-60 (calibration beam spectrum). The k_{Q,Q_0} values for the PTW-34045 and PTW-31010 were obtained from the manufacture published values for the various beam qualities used [66].

The energy dependent correction factors (k_Q) for the PTW-31021 in 6, 9, 12, 18 and 21 MeV electron beams were derived from the absorbed dose to water obtained using the calibrated PTW-34045 plane parallel ionization chamber under reference conditions. The correction factors were calculated using the expression;

$$k_Q = \frac{D^{ref}_{(w,Q,z_{ref})}}{N_{D,w,Q_0} \cdot M_{corr}} \tag{3.12}$$

where

$D^{ref}_{(w,Q,z_{ref})}$ is the absorbed dose to water at reference depth in water for 6, 9, 12, 18 and 21 MeV electron beams measured with the reference detector (PTW-34045) as defined by equations 3.10 under reference conditions, M_{corr} is the charge reading measured with the PTW-31021 under the same reference conditions corrected for all relevant influence quantities and N_{D,w,Q_0} is the absorbed dose to water calibration factor for the PTW-31021 determined in a Cobalt-60 beam under reference condition.

Non-standard photon beams

For machines that cannot realize the reference field of 10 x 10 cm^2 and are used to deliver doses of ionizing radiation using small fields such as in stereotactic radiosurgery, the IAEA TRS-483 CoP recommends performing reference dosimetry measurements in the machine specific reference (msr) field. In this work, a virtual msr field of 6 x 6 cm^2 field was chosen to represent a machine that cannot realize a 10 x 10 cm^2 field. The PTW-30013 was verified to meet the requirement of equation 2.16 for the selected virtual msr field in both 6 and 18 MV beams following recommendations from TRS-483 CoP [22]. The energy dependence correction factor for the PTW-31021 was determined using the formalism;

$$k_{Q,Q_0}^{f_{msr}} = \frac{N_{D,w,Q_{msr}}^{f_{msr}}}{N_{D,w,Q_0}^{f_{ref}}} \tag{3.13}$$

$$= \frac{D_{w,Q_{msr}}^{f_{msr}} / M_{Q_{msr}}^{f_{msr}}}{N_{D,w,Q_0}^{f_{ref}}} \tag{3.14}$$

Where

$N_{D,w,Q_{msr}}^{f_{msr}}$ and $N_{D,w,Q_0}^{f_{ref}}$ are the absorbed dose to water calibration factors for the PTW-31021 in the msr field (f_{msr}) at the user beam and in the reference field (10 x 10 cm^2) at the calibration beam (Cobalt-60) respectively. $M_{Q_{msr}}^{f_{msr}}$ is the integrated charge readings acquired using the PWT-31021 in the msr field corrected for all relevant influence quantities, and $D_{w,Q_{msr}}^{f_{msr}}$ is the absorbed dose to water measured with the reference detector (PTW-30013) in the msr field using the formalism;

$$D_{w,Q_{msr}}^{f_{msr}} = M_{Q_{msr}}^{f_{msr}} N_{D,w,Q_0}^{f_{ref}} k_{Q,Q_0}^{f_{ref}} k_{Q_{msr},Q_0}^{f_{msr}f_{ref}} \tag{3.15}$$

where

$M_{Q_{msr}}^{f_{msr}}$ is the charge reading acquired in the msr field (6 x 6 cm^2) using the PTW-30013 reference detector corrected for influence conditions, recombination and polarity, $N_{D,w,Q_0}^{f_{ref}}$ is the absorbed dose to water calibration factor in a Cobalt-60 beam for the PTW-30013 provided by the calibration laboratory traceable to a primary standard, $k_{Q,Q_0}^{f_{ref}}$ is the beam quality correction factor for the PTW-30013 in a reference field of 10 x 10 cm^2 and $k_{Q_{msr},Q_0}^{f_{msr}f_{ref}}$ is a correction factor that corrects for the difference in the electron fluence at the point of measurement between the reference field (10 x 10 cm^2) and the virtual msr field (6 x 6 cm^2) [22].

For the uncertainties reported in the IAEA TRS-483 CoP, the value of $k_{Q_{msr},Q_0}^{f_{msr}f_{ref}}$ is assumed to be unity. The $k_{Q,Q_0}^{f_{ref}}$ factors are provided in the IAEA TRS-483 CoP for a list of ionization chambers recommended for use in msr fields with various beams qualities ($TPR_{20,10}(10)$).

The $TPR_{20,10}(10)$ used to determine the $k_{Q,Q_0}^{f_{ref}}$ was calculated using the formalism;

$$TPR_{20,10}(10) = \frac{TPR_{20,10}(S)+c\,(10-S)}{1+c(10-S)} \tag{3.16}$$

where

$c = (16.15\pm0.12)\times10^{-3}$ is a constant valid for msr square fields who's sides satisfy the condition $4 \leq S \leq 12$ where S is one side of the msr square field in cm.

3.2.7 Field output factor correction factors in small photon fields

For the determination of field output factors in small fields, measurements were performed using a selection of solid state detectors, vented ionization chambers (excluding the PTW-30013 chamber) and the liquid ionization chamber. All the detectors used in this study were detectors recommended for use in small fields with field output factor correction factors provided in the IAEA TRS-483 CoP [22].

All measurements were performed in water in a 6 MV photon beam at a reference depth of 10 cm from the water surface along the beam's central axis using predetermined square set field sizes of 10 x 10, 6 x 6, 4 x 4, 3 x 3, 2 x 2, 1 x 1 and 0.6 x 0.6 cm^2 normalized to the measurements performed in 10 x 10 cm^2.

The field output factors were calculated using the formalism;

$$\Omega_{Q_{clin},f_{ref}}^{f_{clin},f_{ref}} = \frac{M_{Q_{clin}}^{f_{clin}}}{M_{Q_{ref}}^{f_{ref}}}\, k_{Q_{clin},Q_{ref}}^{f_{clin},f_{ref}} \tag{3.16}$$

where

$\Omega_{Q_{clin},Q_{ref}}^{f_{clin},f_{ref}}$ is the field output factor, $M_{Q_{clin}}^{f_{clin}}$ is the integrated charge reading measured in the user beam for the clinical field (small field), $M_{Q_{ref}}^{f_{ref}}$ is the integrated charge readings measured in the user beam for the reference field (10 x 10 cm^2) and $k_{Q_{clin},f_{ref}}^{f_{clin},f_{ref}}$ is the field output factor correction factor found in the CoP for measurements in small static fields.

The field output factors determined using equation 3.16 for a selection of detectors recommended in the IAEA TRS-483 CoP were fitted into an analytical function shown in equation 3.17 as proposed in the work of Sauer and Wilbert to reduce ambiguity and biasness in the measurements [64].

$$\Omega(S) = P_{\infty}\ \frac{S^n}{l^n + S^n} + S_{\infty}(1 - e^{-bs}) \tag{3.17}$$

Where

P_{∞}, S_{∞}, l, n and b are the fitting parameters that were adjusted to maximize the Maximum Likelihood Estimate (MLE) as described by Casar et al [56]. S is the equivalent square field side calculated from the beam profiles of the cross-plane and in-plane direction then computing $S = \sqrt{a \times b}$ where a and b are the field sizes measured from the lateral profiles as full with at half maximum (FWHM) for in-plane and cross-plane respectively.

In the IAEA TRS-483 CoP, the equivalent square field side defined for small fields is denoted as S_{clin} and this refers to the same parameter as $S = \sqrt{a \times b}$ [22].

Using the analytical function with all the fitting parameters, the field output factor can be predicted for any field size. The field sizes measured with the PTW-31021 were then used in the analytical function to predict the associated field output factors. From the predicted field output factors for the specified field sizes the associated field output factor correction factors $\left(k_{Q_{clin},Q_{ref}}^{f_{clin},f_{ref}}\right)$ for the PTW-31021 were calculated using the formalism;

$$\mathrm{k}_{Q_{clin},Q_{ref}}^{f_{clin},f_{ref}} = \frac{\Omega_{Q_{clin}Q_{ref}}^{f_{clin}f_{ref}}}{\left(\frac{M_{Q_{clin}}^{f_{clin}}}{M_{Q_{ref}}^{f_{ref}}}\right)} \quad (3.\ 18)$$

Where

$\Omega_{Q_{clin}Q_{ref}}^{f_{clin}f_{ref}}$ is the field output factor predicted using the analytical function 3.17, $M_{Q_{ref}}^{f_{ref}}$ is the integrated charge readings measured with PTW-31021 in the reference field 10 x 10 cm^2 and $M_{Q_{clin}}^{f_{clin}}$ is the integrated charge reading measured in the fields; 6 x 6, 4 x 4, 3 x 3, 2 x 2, 1 x 1 and 0.6 x 0.6 cm^2.

The variation in the field output factor correction factors with respect to the field size for the PTW-31021 were then fit to an analytical function 3.19 as proposed in the IAEA TRS-483 CoP [22]. The function 3.19 was then used to predict field output factor correction factors for the PTW-31021 in arbitrary square fields that can then be used to compare with values published by Casar et al [70].

$$\mathrm{k}_{Q_{clin},f_{ref}}^{f_{clin},f_{ref}}(s) = \frac{1+d\,.\,e^{-\frac{10-a}{b}}}{1+d\,.\,e^{-\frac{s-a}{b}}} + c\,.(s-10) \quad (3.19)$$

Where

$\mathrm{k}_{Q_{clin},f_{ref}}^{f_{clin},f_{ref}}(s)$ is the field output factor correction factor as a function of the equivalent square field (S), d is a coefficient that can take binary values of +1 or -1 and a, b and c are fitting parameters that were adjusted for the analytical function to fit the measured data.

Chapter 4 Results and Discussion

4.1 Chamber long term stability

The reference dose rate in a Cobalt-60 teletherapy unit was measured at a water equivalent depth of 5 g/m^2 from the surface of a perspex phantom, using a 80 cm source to chamber distance and 10 x 10 cm^2 field size defined at the isocentric plane, and the results are presented in Table 4.1. The data showing the response of the detector measured over a period of 18 months are presented in figure 4.1.

Table 4.1: The data used to perform calibration on the Cobalt-60 teletherapy unit using the Semiflex 3D ionization chamber and IAEA TRS-398 code of practice on 04-Feb-2017. The average charge reading was corrected for shutter time and influence conditions.

Date	M_{avr} (nC)	Ktp	N_{D,w,Q_0} (Gy/nC)	D_{w,z_{ref},Q_0} (cGy/min)
04-Feb-17	1.892 ± 0.002	1.231	0.05803	135.2 ± 0.4

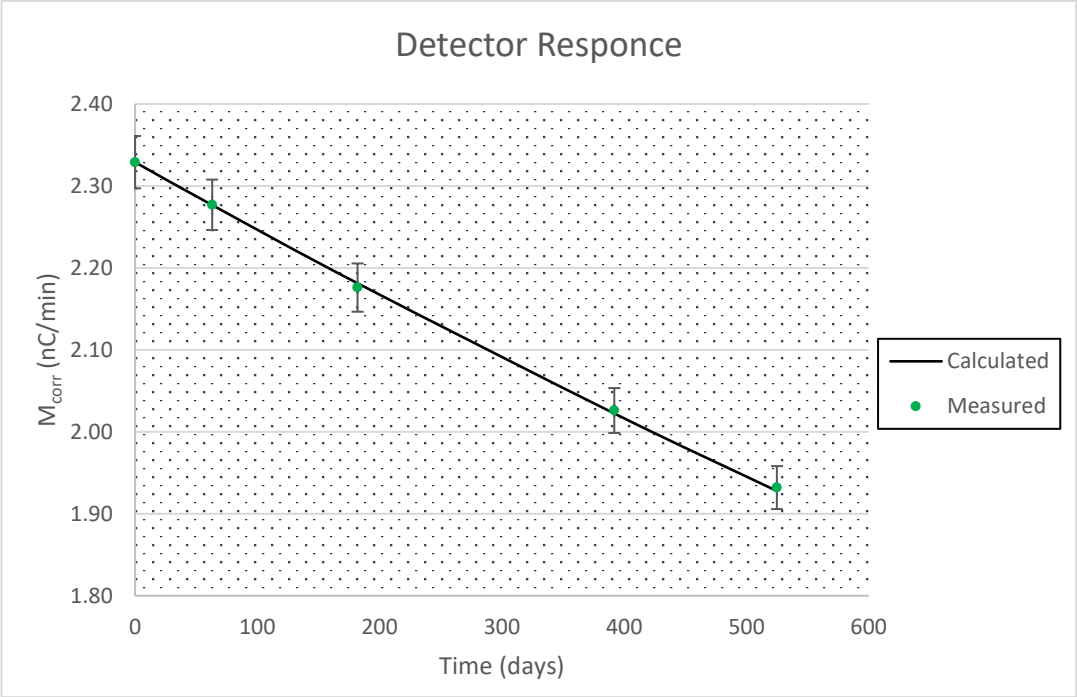

Figure 4.1: The results of the Semiflex 3D ionization chamber stability measurements taken over a period of 18 months.

The results in figure 4.1 shows an average percent difference between the calculated and measured readings of 0.2%. According to the manufacturer's specification, the long term stability of the PTW-31021 is within 0.3% measured over a period of 2 years and according to IEC 60730, the detector long term stability should be within 0.5% [65, 66]. Therefore, the long term stability of the PTW-31021 measured over a period of 18 months was found to be within manufacture specification and internationally recommended standards.

4.2 Chamber response linearity

The linear response of the PTW-31021 was investigated over a range of monitor units (10MU – 640MU). The detector response was measured in terms of integral charge measured under reference conditions at a depth of 10 cm in water and SAD 100 cm. Figure 4.2 shows linear response of the PTW-31021 in 6 and 18 MV beams given by the ratio of the chamber response to delivered monitor unit as a function of delivered

monitor units. A linear regression line was employed for fitting the data and the coefficient of variance was used as a measure of the linear response of the PTW-31021.

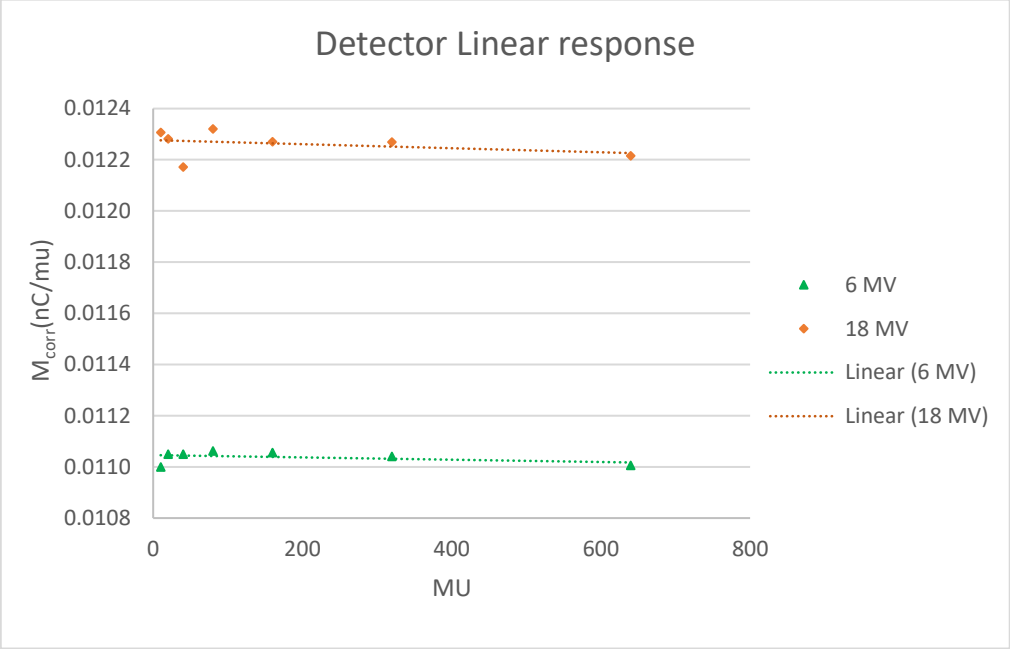

Figure 4.2: The response of the PTW-31021 to delivered monitor units (MU) ranging from10 MU to 640 MU. The graph shows the ratio of the chamber response to delivered monitor unit plotted as a function of MUs. The calculated coefficients of variance were 0.2% and 0.4% for 6 MV and 18 MV respectively.

The linear coefficient calculated as the ratio of the chamber response corrected for influence quantities to delivered monitor units was used as a measure of the ionization chamber response linearity and the standard deviation of the linear coefficients was used to quantitative the linearity of the ionization chamber response. The standard deviation in the linear coefficient was calculated to be: 0.2% and 0.4% for 6 MV and 18 MV, respectively. This is also in line with recommendations of IEC 60730 which recommends 0.5% [65]. Therefore, the linear response of the PTW-31021 measured over the range 10 MU – 640 MU was found to be within internationally recommended standards.

4.3 Verifying the effective point of measurement

The effective point of measurement is an alternative to the displacement correction factor that is used to correct for the water replacement by the detector in the determination of absorbed dose to water [25]. The effective point of measurement for the PTW-31021 was determined by shifting the relative depth ionization curve measured with the PTW-31021 to match that of the PTW-34045. Figure 4.3 shows the relative depth ionization curves of the PTW-34045 and PTW-31021 used to determine the actual effective point of measurement for the PTW-31021.

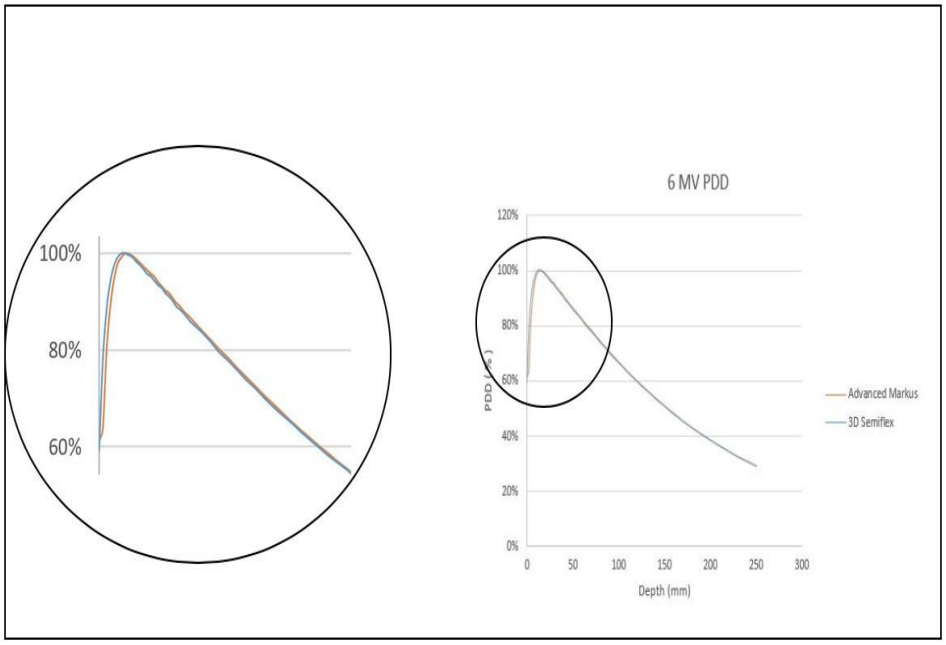

Figure 4.3: The relative depth ionization curves measured with the Advanced Markus compared to that measured with the Semiflex 3D ionization chamber set-up to the recommended effective point of measurement. The Semiflex 3D ionization chamber was oriented perpendicular to the beam. The actual effective point of measurement was determined by displacing the Semiflex 3D ionization chamber data to match the Advanced Markus data.

Figure 4.4 shows the relative depth ionization curve for the PTW-31021 displaced by 1.3 mm to match the PTW-34045 data.

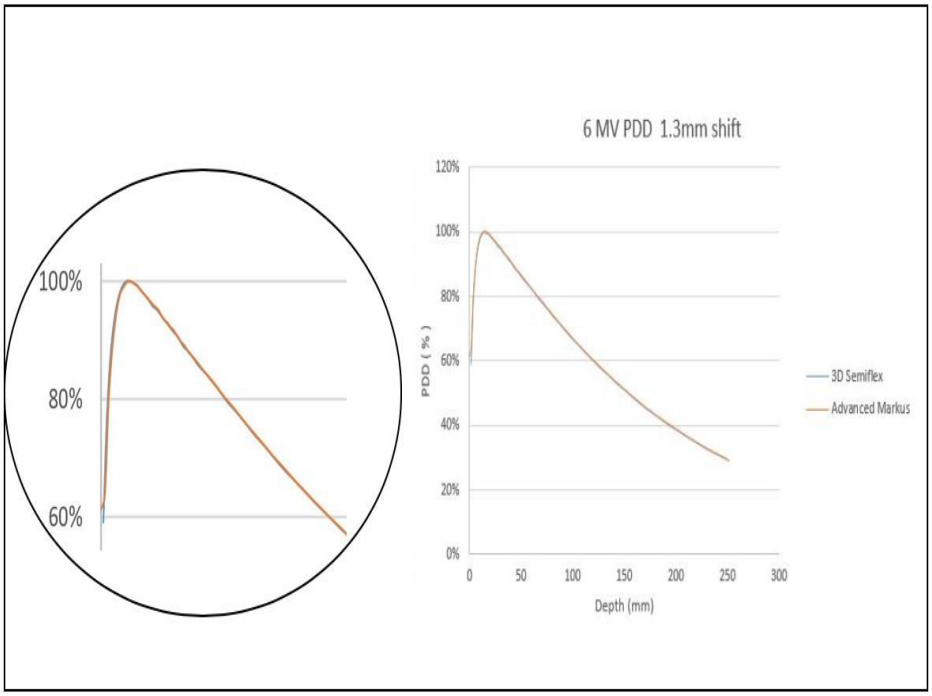

Figure 4.4: A comparison of the relative depth ionization curves for the Semiflex 3D ionization chamber (mounted parallel to the beam axis) and the Advanced Markus. The data for the Semiflex 3D was displaced by 1.3 mm to match that of the Advanced Markus.

The new effective point of measurement was validated using gamma analysis and the agreement between the relative depth ionization curves measured using PTW-3102and PTW-34045 was quantify the agreements. Figure 4.5 shows the gamma analysis comparing PTW-34045 to PTW-31021. The distance to agreement (DTA) and the dose tolerance were set to 1 mm and 1.5% respectively.

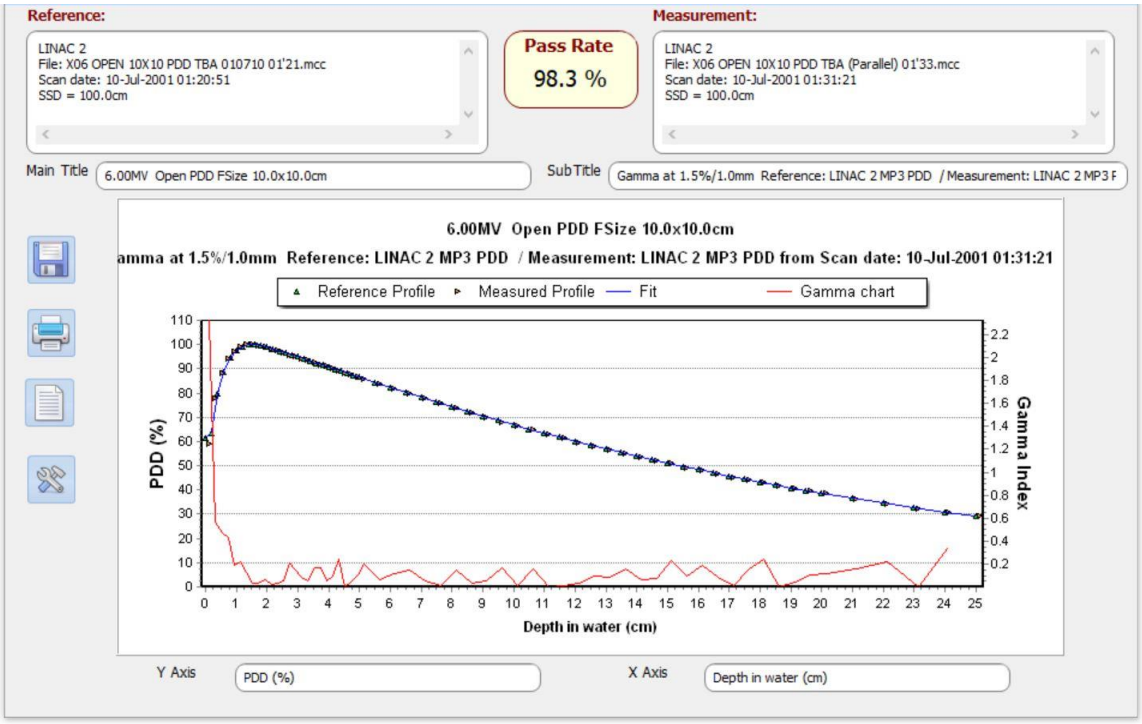

Figure 4.5: Results from the gamma analysis, in which the relative depth ionization curve acquired using the Advanced Markus chamber was used as a reference and compared with the relative depth ionization curve acquired using the Semiflex 3D ionization chamber mounted parallel to the beam axis. The relative depth ionization curve of the Semiflex 3D ionization chamber was shifted by 1.3 mm away from the source.

When the PTW-31021 was mounted perpendicular to the beam central axis, the displacement of the EPOM from the reference point defined by the manufacture was found to be 1.4 ± 0.1 mm towards the source and when the chamber was mounted parallel to the beam axis, the displacement of the EPOM was 1.3 ± 0.1 mm up-stream towards the chamber tip along the chamber axis from the reference point defined by the manufacture.

The gamma analysis tool was used to validate the shift used to match the relative depth ionization curves acquired using the PTW-34045 to that acquired with the PTW-31021. The gamma index method quantitatively evaluates the agreement between the reference PDD (PTW-34045) and the measured PDD (PTW-31021) after the applied shift by calculating the percent difference in dose for the two profiles at various points with similar special coordinates (distance to agreement). The pass criterion was set to 1 mm distance to agreement and 1.5% dose tolerance. This meant, at each evaluation

point the percent dose difference between the refence PDD profile and the measured PDD profile needed to be withing 1.5% and the coordinates of the evaluation points needed to agree to within 1mm. The results showed very good agreement between the reference and the PTW-31021 data with 98.3% and 100% of the evaluated points meeting the requirements for the parallel and perpendicular orientations of the PTW-31021 respectively. Relatively large deviations were observed at deeper depths and the possible causes of these deviation is most likely a low signal to noise ratio at very low dose rates for the PTW-31021. From these results, we can conclude that the reference point recommended by the manufacture is different from the EPOM for the PTW-31021.

4.4 Pre-irradiation and post-irradiation leakage current

The PTW-31021 pre and post irradiation leakage current was measured in a 6 MV beam using 10 cm and 20 cm square set fields defined at the isocenter. The measurements were performed in water at a reference depth of 10 cm and the results are displayed in table 4.2

Table 4.2: The results of pre-irradiation and post-irradiation leakage tests performed on the Semiflex 3D ionization chamber using 6 MV photon beam, $10cm \times 10cm$ and $20cm \times 20cm$ fields and 1 minute intervals.

	Pre-irradiation(%)	Post irradiation(%)
$10cm \times 10cm$	0.001 ± 0.0004	0.005 ± 0.0002
$20cm \times 20cm$	0.003 ± 0.001	0.026 ± 0.003

The results showed pre and post irradiation leakage current of the order of 0.003% and 0.03%, respectively. This is well below the 0.5% limit as recommended in IEC 60731 guidelines [65]. Therefore the pre and post irradiation leakage current for the PTW-31021 in a 6 MV beam was found to be in very good agreement with international recommendations [65].

4.5 Beam quality dependence

The energy dependence of the PTW-31021 was investigated by comparing the dose rates measured with the PTW-31021 in different photon and electron beam qualities to that measured with reference detectors of known energy dependence.

Standard Photon beams

Figure 4.6 shows the results of response of the PTW-31021 compared to the dose rate measurements of the PTW-30013 and PTW-31010 in Cobalt-60, 6 and 18 MV photon beam qualities.

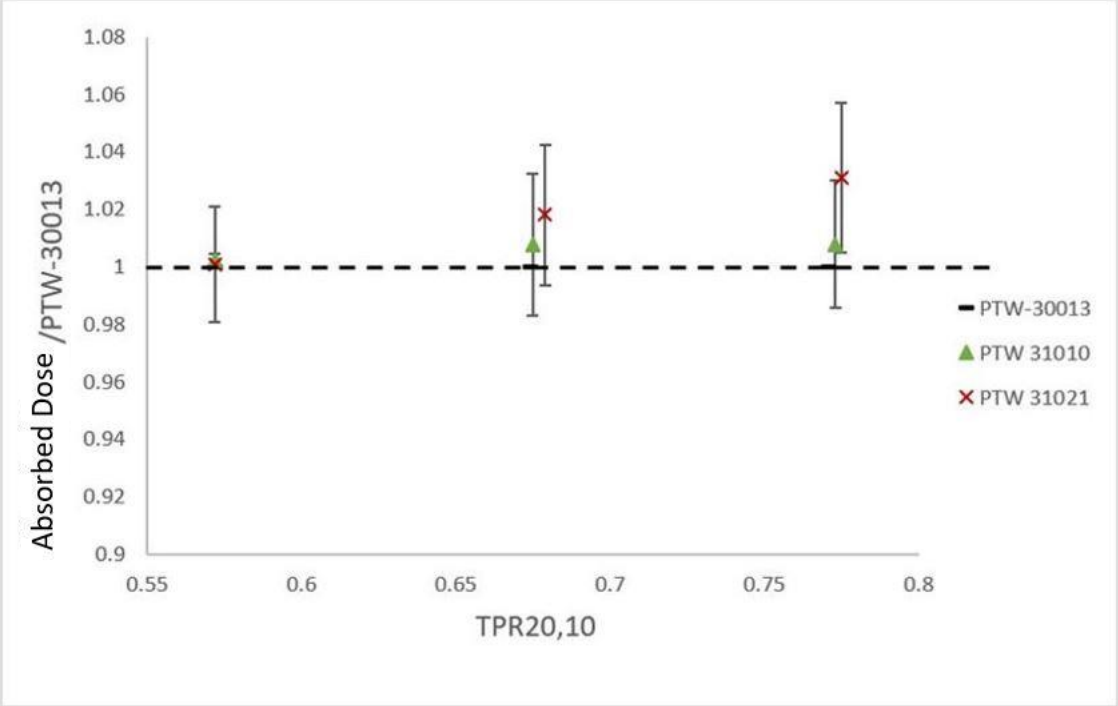

Figure 4.6: The relative dose obtained as a function of beam quality measured in three photon beams performed with three different detectors normalized to PTW-30013. The PTW-30013 Farmer chamber, PTW-31010 Semiflex and PTW-31021 Semiflex 3D Ionization chamber were mounted perpendicular to the beam axis. The results were normalized to the dose rate measurements obtained with the PTW-30013.

The response of the PTW-31021 when compared to the absorbed dose rate measured with PTW-30013 indicates that the response of PTW-31021 is influenced by beam quality. The calculated k_{Q,Q_0} values to correct the response of PTW-31021 for the difference in the beam quality between the calibration and the user beam are given in table 4.3. The beam quality correction factors were assumed to be independent of the chamber orientation.

Table 4.3: Beam quality correction factors (k_{Q,Q_0}) for a PTW-31021 determined in 6 and 18 MV photon beams from measurements performed in a conventional field size 10 x 10 cm^2. The correction factors were determined for measurement with a PTW-31021 mounted perpendicular to the beam axis against measurements with a PTW-30013 under identical conditions. The estimated uncertainty is 3.6 % at k = 2.

	6 MV	**18 MV**
K_Q	0.991	0.973
$TPR_{20,10}(10)$	0.679	0.775

Standard electron Beams

The energy dependence of the PTW-31021 was also investigated in 12, 18 and 21 MeV electron beams by comparing the PTW-31021 response to the absorbed dose rate measured with the PTW-34045 and PTW-31010. Figure 4.7 shows the results of the response of the PTW-31021 compared to the dose rate obtained with the PTW-31010 and PTW-34045 as a function of electron beam quality (R_{50}).

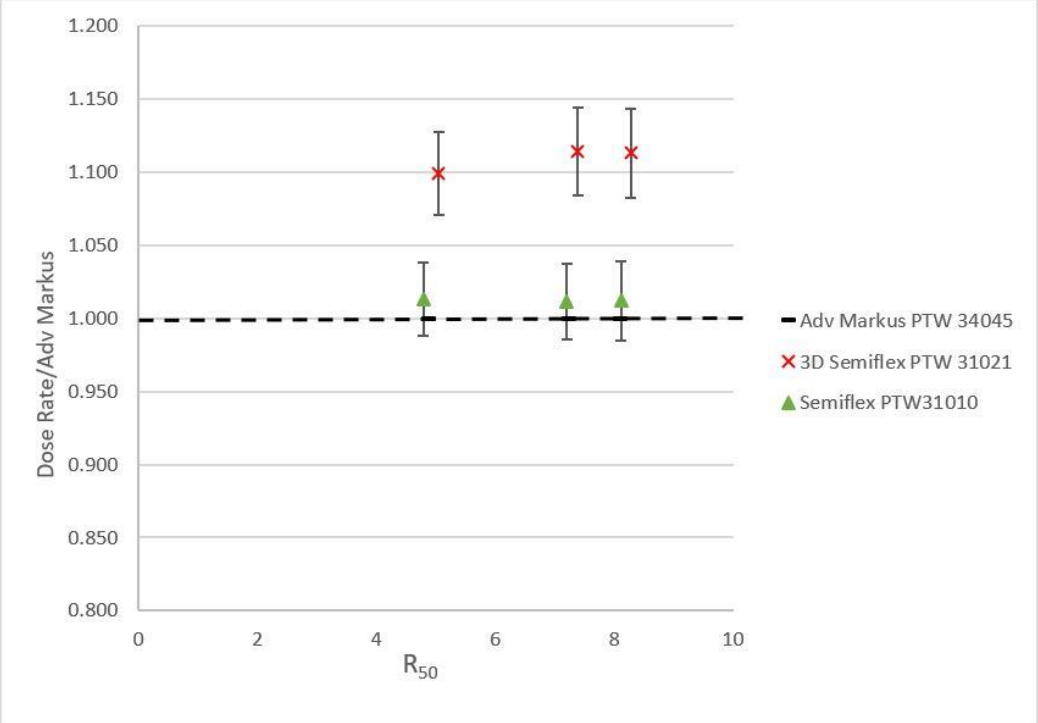

Figure 4.7: Measurements used to determine electron beam quality correction factors for PTW-31021 using absorbed dose rate data obtained with PTW-34045 and PTW-31010 detectors. All measured dose rates were normalized to the values obtained using the PTW-34045.

The measured k_{Q,Q_0} values of the PTW-31021 ion chamber are provided in table 4.4.

Table 4.4: Beam quality correction factors (k_{Q,Q_0}) for PTW-31021 determined in electron beams of various electron beam qualities (R_{50}) from measurements performed under reference conditions. The PTW-31021 was mounted perpendicular to the beam axis. The correction factors were determined against measurements performed with a PTW-34045 under identical conditions. The estimated uncertainty is 3.8% at k = 2.

	6 MeV	9 MeV	12 MeV	18 MeV	21 MeV
k_Q (PTW-31021)	0903	0.921	0.899	0.905	0.895
k_Q (PTW-31010)	-	-	0.909	0.900	0.898
R_{50} (g/cm^2)	2.57	3.82	5.04	7.39	8.28

The k_Q values for PTW-31021 determined in this study for electron beams have been regarded as new values and there were no published values available for comparison at the time of writing this dissertation. The manufacture does not recommend the use of PTW-31021 in electron beams with average energy less than 9 MeV and the IAEA TRS-398 CoP also does not recommend the use of cylindrical ionization chambers for reference dosimetry in electron beams with average energy less than 10 MeV.

Nonstandard photon beams

The $k_{Q,Q_0}^{f_{msr}}$ values measured in a 6 x 6 cm^2 msr field are presented in table 4.5 as a function of $TPR_{20,10}(10)$.

Table 4.5: Beam quality correction factors for PTW-31021 measured in 6 and 18 MV photon and a 6 x 6 cm^2 "virtual" msr field. The $k_{Q,Q_0}^{f_{msr}}$ values were determined from measurements against PTW-30013. The estimated uncertainty is 3.8% at k = 2.

	6 MV	**18 MV**
$k_{Q,Q_0}^{f_{msr}}$	1.006	0.975
$TPR_{20,10}(10)$	0.680	0.77

The use of PTW-30013 in a 6 x 6 cm^2 msr field and photon beams with beam qualities $TPR_{20,10}$ = 0.68 and 0.77 was found to satisfy the condition FWHM ≥ 2 * r_{LCPE} + d.

4.6 Field output correction factors in small photon fields

The analytical function of Sauer and Wilbert [64] was used to fit field output factors measured with a selection of solid state detectors and vented ionization chambers recommended for use in small static fields in the IAEA TRS-483 CoP [22]. The fitting parameters that produced the best fit for the analytical function were: $P_{\infty} = 0.741$, $S_{\infty} = 0.41$, $l = 0.517$, $n = 2.433$ and $b = 0.099$. The analytical function was then used to predict the field output factor for a range of equivalent square field sizes (S_{clin}). The predicted field output factors and the response of the PTW-31021 in a range of selected field sizes were then used to calculate the field output factor correction factors ($k_{Q_{clin},Q_{ref}}^{f_{clin},f_{ref}}$) for the PTW-31021 as a function of S_{clin}. The overall uncertainty in the field output factor correction factors were found to be within 1.8% except for the 0.6 x 0.6 cm^2 field size with an estimated uncertainty of 2.6%. Table 4.5 provides the calculated field output factor correction factors for the PTW-31021 and the published field output correction factors for all the other small field detectors used in this study, as obtained from the IAEA TRS-483 CoP excluding PTW-30013.

Table 4.6: The field output factor correction factors ($k_{Q_{clin},Q_{ref}}^{f_{clin},f_{ref}}$) as a function of S_{clin} in a 6 MV beam with flattening filter for a selection of detectors that were used in the study for measurement in small fields. The correction factors for the PTW-31021 were determined in this study and the correction factors for all the other detectors used in this study were obtained from the IAEA TRS-483 Cop [22].

S_{clin} *(cm)*	Semiflex 3D PTW-31021 (perp)	Semiflex 3D PTW-31021 (parallel)	Diode PTW-60012	Micro Diamond PTW-60019	Semiflex PTW-31010	Pin Point 3D PTW-31016	MicroLion PTW-31018
8.0	1.000	1.000	1.005	1.000	1.000	1.000	0.997
6.0	1.000	1.000	1.010	1.000	1.000	1.000	0.994
4.0	0.999	0.999	1.015	1.000	1.000	1.000	0.991
3.0	0.999	0.999	1.017	1.000	1.001	1.001	0.989
2.5	1.000	1.000	1.017	0.999	1.002	1.001	0.988
2.0	1.002	1.001	1.016	0.997	1.008	1.004	0.988
1.5	1.012	1.010	1.010	0.993	1.025	1.013	0.987
1.2	1.033	1.029	1.003	0.989	-	1.025	0.987
1.0	-	-	0.996	0.984	-	1.039	0.987
0.8	-	-	0.985	0.977	-	-	0.990
0.6	-	-	0.970	0.968	-	-	0.999
0.5	-	-	0.960	0.962	-	-	1.011
0.4	-	-	-	0.955	-	-	1.033

Figure 4.9 shows a graphical representation of all the field output factors measured in this study for a range of small field sizes.

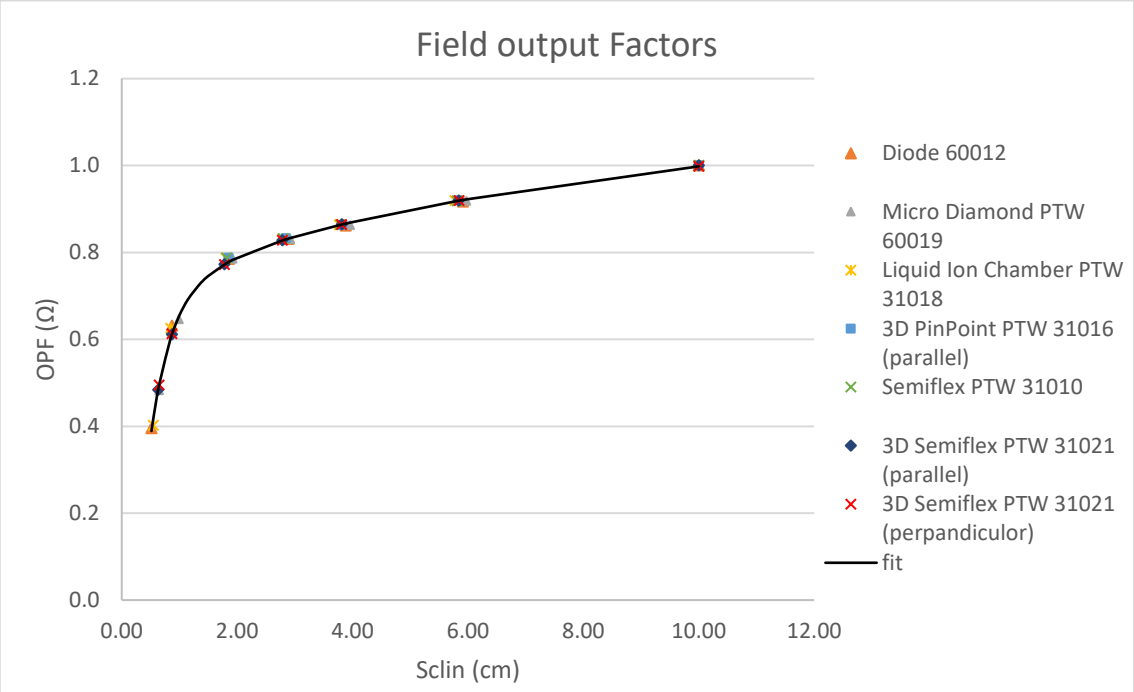

Figure 4.9: Field output factors measured in small static fields using a relatively large selection of detectors. The field output factors were fitted to an analytical function to produce the line of best fit represented by the solid black line.

The analytical function $k_{Q_{clin},Q_{ref}}^{f_{clin},f_{ref}}(s) = \frac{1+d\,.\,e^{-\frac{10-a}{b}}}{1+d\,.\,e^{-\frac{s-a}{b}}} + c\,.(s-10)$ proposed in the IAEA TRS-483 CoP was then used to obtain the calculated field output factor correction factors for the PTW-31021 in any arbitrary square field (S). The fitting parameters that produced the best fit for the function were; a = 0.120, b = 0.304, c = 9.00 × 10^{-5} and d = -1 when the PTW-31021 was mounted parallel to the beam axis and a = 0.140, b = 0.310, c = 9.00 × 10^{-5} and d = -1 when the PTW-31021 was perpendicular to the beam axis. The results of the analytical function fitted to the calculated field output factor correction factors obtained from measurements performed with the PTW-31021 mounted perpendicular and parallel to the beam axis are presented in figure 4.10. and 4.11.

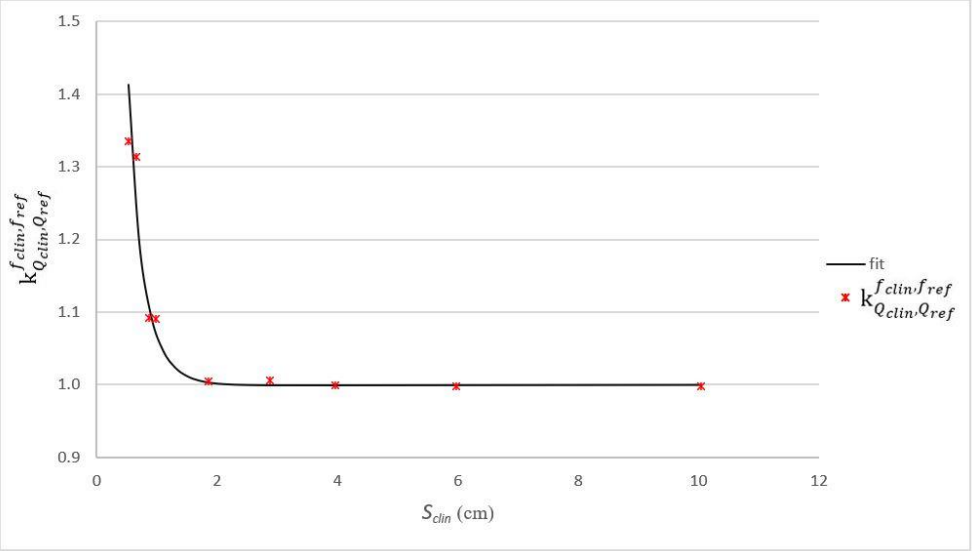

Figure 4.10: Field output factor correction factors $k_{Q_{clin},Q_{ref}}^{f_{clin},f_{ref}}$ for PTW-31021 (mounted perpendicular to the beam axis) as a function of S_{clin} (cm) fitted to an analytical function proposed in the IAEA TRS-483 CoP [22].

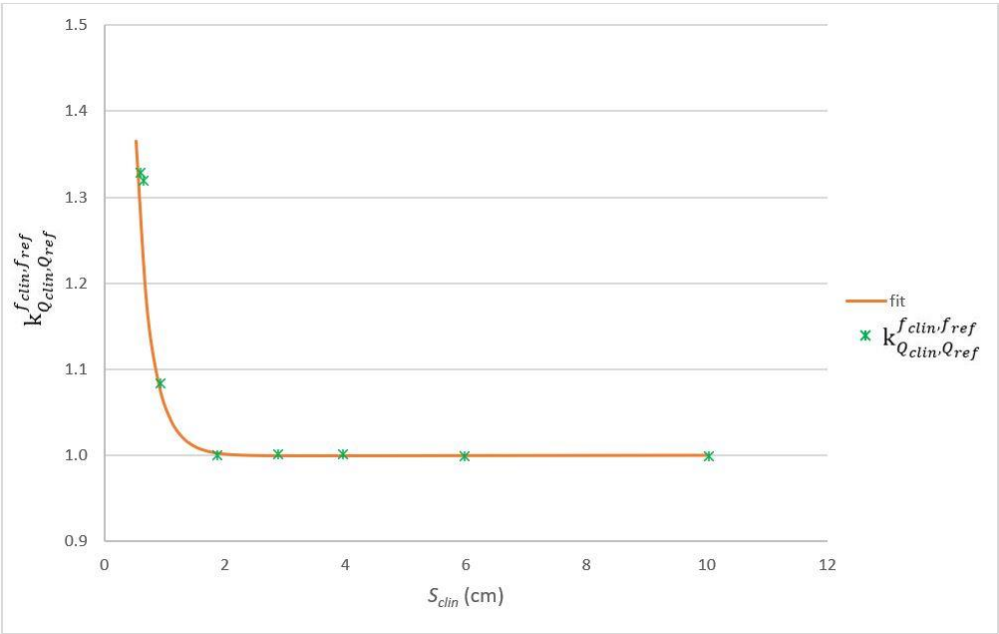

Figure 4.11: Field output factor correction factors $k_{Q_{clin},Q_{ref}}^{f_{clin},f_{ref}}$ for PTW-31021 (mounted parallel to the beam axis) as a function of S_{clin} (cm) fitted to an analytical function proposed in the IAEA TRS-483 CoP [22].

The estimated field output factor correction factors $\left(k_{Q_{clin},Q_{ref}}^{f_{clin},f_{ref}}\right)$ for the PTW-31021 for both orientations are presented in figure 4.12 plotted as a function of S_{clin}. The graph also includes the field output factor correction factors for all the other small field detectors that were used in this study, as obtained from the IAEA TRS-483 CoP [22].

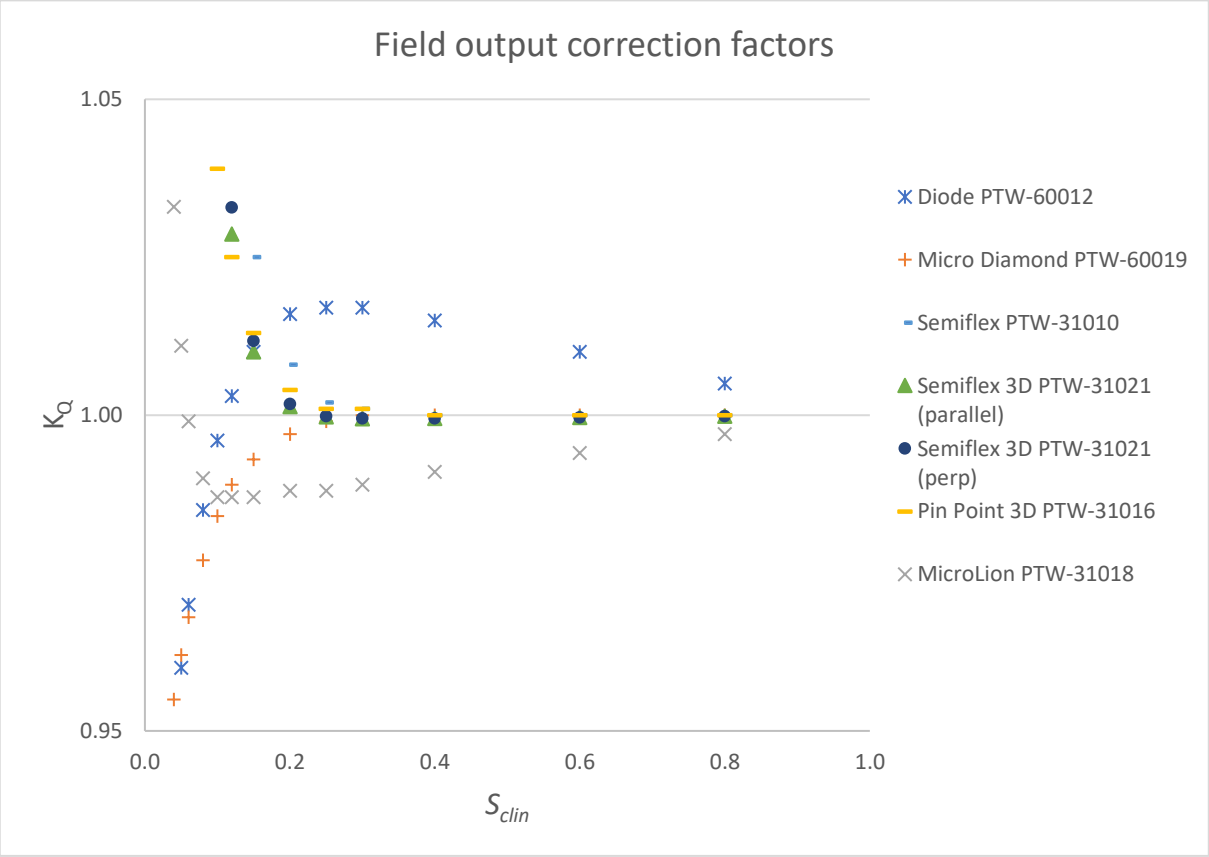

Figure 4.12: Field output factor correction factors for the detectors used for small field output factor measurements as a function of the equivalent square field (S_{clin}). The field output factor correction factors determined for the PTW-31021 in the perpendicular and parallel orientation are also shown.

The results of this study suggest that the smallest S_{clin} in which the PTW-31021 is recommended to be used is 1.2 cm. Below this field size, the field output factor correction factors become larger than 5 %, which is recommended as the upper limit [55]. This is in agreement with the findings of Casar, et al who suggest that

the smallest field size in which the PTW-31021 can be used, lies between 1.5 x 1.5 cm^2 and 1 x 1 cm^2 [70].

Table 4.7: A comparison of the field output factor correction factors for PTW-31021 determined in this study (CMJAH) to that of Casar et al. in 6 MV WFF [70]. The values in brackets shows the uncertainty (reported to 1 standard deviation) in the last one or two digits.

	Semiflex 3D PTW-31021 (parallel)		**Semiflex 3D PTW-31021 (perpendicular)**	
S_{clin} **(cm)**	**CMJAH**	**Casar et al.**	**CMJAH**	**Casar et al.**
0.5	1.400 (42)	1.394(23)	1.454 (22)	1.461(25)
0.8	1.119(51)	1.145(10)	1.134(15)	1.157(10)
1.0	1.058(0)	1.075(8)	1.065(6)	1.077(8)
1.5	1.010(2)	1.021(6)	1.012(7)	1.020(6)
2.0	1.001(2)	1.007(6)	1.002(3)	1.008(6)
3.0	0.999(3)	1.000(6)	0.999(3)	1.001(6)
4.0	0.999(2)	0.998(6)	0.999(1)	0.999(6)
5.0	1.000(1)	0.999(6)	1.000(1)	1.000(6)
10.0	1.000(0)	1.001(1)	1.000(0)	1.001(0)

Chapter 5 Conclusions

The dosimetric performance of a new 3D air ionization chamber designed for use in standard and nonstandard fields, was investigated. The characteristics of the ionization chamber were quantified in terms of its long term stability, linear response with absorbed dose, effective point of measurement, pre- and post-irradiation leakage current, beam quality dependence in both photon and electron beams, as well as beam quality dependence correction factors and field output factor correction factors in small static fields using a 6 MV flattened photon beam.

- The chamber long term stability was investigated by measuring the dose rate from a Cobalt-60 teletherapy beam over an 18 month period and the result were found to be in good agreement with manufacture specifications and recommendations in IEC 60731 [65].
- The ionization chamber demonstrated a linear response for a range of absorbed dose to water in 6 and 18 MV photon beams. The coefficient of variance calculated for the ratio of chamber response to delivered monitor units was found to be less than 0.5% for doses of up to approximately 5.04 Gy.
- The effective point of measurement is displaced from the reference point specified by the manufacture. The displacement was found to be 1.3 ± 0.1 mm up stream from the manufacture defined reference point for the parallel orientation and 1.4 ± 0.1 mm towards the source for the perpendicular orientation.
- The pre- and post-irradiation leakage current for the PTW-31021 was investigated in a 6 MV beam using 10 x 10 cm^2 and 20 x 20 cm^2 square fields. The results were well below the 0.5 % recommendation in IEC 60731 guidelines [65]. In this study, measurements of lateral beam profiles and polarity correction factors for various “large” field sizes were not performed in order to determine the effect of cable and stem irradiation in large fields. This could result in radiation induced leakage current

that introduces errors in chamber response of the order of ± 5 % and requires further investigation.

- The experimentally determined correction factors for beam quality dependence (k_Q) in standard high energy photon and electron beams were comparable to the values published by the manufacture however, the estimated uncertainties were significantly higher in comparison to values published by the manufacture [66]. The PTW-31021 and PTW-31010 resulted in different beam quality correction factors measured. This can be accredited to the difference in the design of the two chambers, with PTW-31010 and PTW-31021 having sensitive volumes of 0.125 cc and 0.07 cc, respectively.
- For measurements in nonstandard small fields, due to the relatively large outer diameter of the detector in comparison to the size of the sensitive volume, the PTW-31021 does not provide an advantage for reference dosimetry measurements in msr fields when compared to the PTW-31010.
- The PTW-31021 does however produce better performance in relative dosimetry measurements (e.g. field out-put factors measurements) in small fields compared to the PTW-31010 due to its smaller active volume of 0.07cc compared to 0.125 cc of the PTW-31010. The manufacturer specifications recommend that the smallest field size that can be used with PTW-31021 is 2.5 x 2.5 cm^2. The results of this study suggest that the smallest field size in which the PTW-31021 could be used lies somewhere between 1.2 x 1.2 cm^2 and 1 x 1 cm^2 Compared to the 1.5 x 1.5 cm^2 of the PTW-31010. This is also in agreement with the data published by Casar, et al. [70]. Considering the active volume of PTW-31021 compared to the PTW-31010 or the PTW 31016, the results of this study are also in agreement with the data published in the IAEA TRS-483 CoP [22].

Bibliography

(1) **B. Edwards, V. Clarke**, *The psychological impact of a cancer diagnosis on families: the influence of family functioning and patients illness characteristics on depression and anxiety*. Psycho-Oncology, 2004, **1**: 562–576.

(2) **A. Miller, I. Salas, A. Haden**, *Cancer control: Knowledge in action, WHO guide for effective programmes*. World Health Organization, CH- 1211 Geneva 27, Swidzerland, 2007.

(3) **T. M. Buzug,** *Computed Tomography, from photon statistics to modern cone-beam CT*. Springer, Verlag Berlin Heidelberg, 2008.

(4) **A. Herskovic, K. Martz, M. Al-Sarref, L. Leichman, J. Brindle, et al.**, *Combined chemotherapy and radiotherapy compared with radiotherapy alone in patients with cancer of the esophagus*. The new England Journal of Medicine, 1992, **326**: 1593– 1598.

(5) **B. A. Tisdale**, *When to consider radiation therapy for your patients*. American Family Physicist, 1999, **59**: 1177–1184.

(6) **S. Martino, T. G. Odle**, *Advanced practice in radiation therapy*. American Society of Radiation Technologists: Albuquerque, NM, 2007.

(7) **P. Hoskin**, *External Beam Therapy*. Oxford University Press, **2nd**, UK, 2012.

(8) **D. Thwaites**, *7th International Conference on 3D Radiation Dosimetry*. Journal of Physics, 2013.

(9) **Rossi, H. Harald**, *Radiation Physics and Radiobiology*. Health Physics, 1996, **6**: 828–831.

(10) **E. C. Halperin, C. A. Perez, L. W. Brady**, *Principles and Practice of radiation oncology*. **5th ed**., Lippincott-Raven, Philadelphia, 2004.

(11) **K.-A. Johansson, S. Mattsson, A. Brahme, J. Carlsson, B. Zackrisson**, *Radiation therapy dose delivery*. Acta Oncologica, 2003, **42**: 85–91.

(12) **J. E. Lye, D. J. Butler, C. P. Oliver, A. Alves, J. Lehmann, F. P. Gibbons, I. M. Willians**, *Comparison between the TRS-398 code of practice and the TG-51 dosimetry protocol for flattening filter free beams*. Physics in Medicine and biology, 2016, **61**: 362–372.

(13) **J. Thariat, J.-M. Hannoun, A. S. Myint, T. Vuong and J.-P. Gerard**, *Past, present and future of radiotherapy for the benefit of patients*. Nature Review Clinical Oncology, 2013, **10**: 52–60.

(14) **I. J. Das, G. X. Ding, A. Ahnesjo**, *Small fields: Nonequilibrium radiation dosimetry*. American Association of Physicist in Medicine, 2008, **35**: 206– 2015.

(15) **E. Benitez, F. Casado, S. Garcia-Pareja, J. Martin-Viera, C.Moreno, V.parra**, *Evaluation of a liquid ionization chamber for relative dosimetry in small and large fields of radiotherapy photon beams*. Radiation Measurements, 2013, **58**: 79–86.

(16) **N. Ade, T. Nam, T. Derry, S. Mhlanga**, *The dose rate dependence of synthetic diamond detectors in the relative dosimetry of high-energy electron therapy beams*, Radiation physics and chemistry. 2014, **98**: 155– 162.

(17) **N. Ade, T. Nam**, *The influence of detector size relative to field size in small-field photon beam dosimetry using synthetic diamond crystals as sensors*. Radiation physics and chemistry, 2015, **113**: 6–13.

(18) **I. Das, G. Ding, A. Ahnesjo**, *Small fields: Nonequilibrium radiation dosimetry*. AAPM Medical Physics, 2008, **35**: 562–576.

(19) **H. F. Godson, M. Ravikumar, K. Ganesh, S. Sathiyan, Y. R. Ponmalar**, *Small field output factors: Comparison of measurements with various detectors and effects of detector orientation with primary jaw setting.* Radiation Measurements, 2016, **85**: 99–110.

(20) **S. H. Benedict, D. J. Schlesiger, S. J. Goetsch**, *Stereotactic Radiosurgery and Stereotactic body radiation therapy*. Taylor and Francis, Florida, 2016.

(21) **W. Parwaie, S. Refahi, M. A. Ardekani, B. Farhood**, *Different dosimeters/ detectors used in small-field dosimetry: Pros and cons*. J Med Sign Sens 2018, **8**: 195-203.

(22) **H. Palmans, P. Andreo, M. S. Huq, J. Seuntjens, K. E. Christaki, A. Meghzifene**, *Dosimetry of small static fields used in external photon beam*

radiotherapy TRS-483, the IAEA–AAPM international Code of Practice for reference and relative dose determination. Medical Physics, 2018, **45**: e1123–e1145.

(23) **E. B. Podgorsak**, *Radiation Oncology Physics: A Handbook for Teachers and Students*. International Atomic Energy Agancy, Vienna, Austria, 2005.

(24) **P. R. Almond, P. J. Biggs, B. M. Coursey, W. F. Hanson, M. S. Huq, R. Nath, D. W. O. Rogers**, *AAPM's TG-51 protocol for clinical reference dosimetry of high-energy photon and electron beams*. Med., Phys., 1999, **26**: 1847-1870. doi:10.1118/1.598691

(25) **International Atomic Energy Agency (IAEA)**, *Absorbed Dose Determination in External Beam Radiotherapy: An International Code of Practice for Dosimetry based on Standards of Absorbed Dose to Water*. Technical Report Series **398**, version 12, IAEA, Vienna, Austria, 2000.

(26) **C. C. Thomas**, *The Physics of Radiology*. Springfield, Illinois, USA, **4th ed.**, 1983.

(27) **J. R. Greening**, *Fundamentals of Radiation Dosimetry*. Taylor and Francis, London, **2nd ed.**, 1985.

(28) **F. M. Khan**, *Handbook of the Physics of Radiation Therapy*. Lippincott Williams and Wilkins, **4th ed.**, Philadelphia, USA, 2010.

(29) **R. Waggener, J. Kereiakes, R. Shalek**, *Handbook of Medical Physics*. CRC Press, 1984.

(30) **P. Mayles, A. Nahum, J. C. Rosenweld**, *Handbook of Radiotherapy Physics, Theory and Practice*. Taylor and Francis group LLC, New York, 2007.

(31) **J. H. Hubbell**, *Review of photon interaction cross section data in the medical and biological context*. Physics in Medicine and Biology, 1999, **44**: R1–R22.

(32) **A. E. Nahum**, *Water/ air mass stopping power ratios for megavoltage photon and electron beams*. Physics in Medicine and Biology, 1978, **23**: 24–38.

(33) **C. Goma, P. Andreo, J. Sempau**, *Spencer-Attix water/medium stoppingpower ratios for the dosimetry of proton pencil beams.* Physics in Medicine and Biology, 2013, **58**: 2509–2522.

(34) **T. Kron, J. Lehmann, P. Greer**, *Dosimetry of ionizing radiation in modern radiation oncology*. Physics in Medicine and Biology, 2016, **61**: 167–205.

(35) **P. Andreo**, *Dose to water-like media or dose to tissue in MV photon radiotherapy treatment planning: still a matter of debate*, Physics in Medicine and biology, 2015, **60**: 309–337.

(36) **P. Almond, H. Svensson**, *Ionization Chamber Dosimetry for Photon and Electron Beams*. **tech. rep.**, University of Texas, 2009.

(37) **G. Shani**, *RADIATION DOSIMETRY Instrumentation and Methods*. CRC Press LLC, United State of America, **2nd .ed**, 2001.

(38) **M. C. Ma, C. W. Coffey, L. A. DeWerd, R. Liu, C. nad Nath, M. S. Seltzer, J. P. Seuntjens**, *AAPM protocol for 40-300 kV X-ray beam dosimetry in radiotherapy and radiobiology.* The International Journal of Medical physics Research and Practice, 2001, **28**: 1141–1144.

(39) **F. Attix**, *Introduction to Radiological Physics and Radiation Dosimetry.* John Wiley and Sons, Inc., **1st ed.**, 1986.

(40) **ICRU**, *Key Data for Ionizing-Radiation Dosimetry: Measurement Standard and Applications*. Report 90, 2016.

(41) **P. Andreo, D. T. Burns, A. E. Nahum, J. Seuntjens, F. H Attix**, *Fundamentals of Ionizing Radiation Dosimetry*. John Wiley and sons, Inc., 2017.

(42) **H. Bouchard, J. Seuntjens, J.-F. Carrier, I. Kawrakow**, *Ionization chamber gradient effects in nonstandard beam configurations*. Med. Phys., 2009, **36**: 4654-4663. doi:10.1118/1.3213518

(43) **ICRU**, *Determination of Absorbed Dose in a Patient Irradiated by Beams of X or Gamma rays in Radiotherapy Procedures*. Report 24,1976

(44) **AAPM Protocol Task Group 21**: *A protocol for the determination of absorbed dose from high-energy photon and electron beams*. Med. Phys., 1985, **10**: 741-771

(45) **M. S. Huq, H. Song, P. Andreo, C. J. Houser**, *Reference dosimetry in clinical high-energy electron beams: Comparison of the AAPM TG-51 and AAPM TG-21 dosimetry protocols.* Med. Phys., 2001, **28**: 2077-2087. doi:10.1118/1.1405841

(46) **A. Sarfehnia, B. Clasie, E. Chung, H. M. Lu, J. Flanz, E. Cascio, M. Engelsman, H. Paganetti, J. Seuntjens**, *Direct absorbed dose to water determination based on water calorimetry in scanning proton beam delivery*. Med. Phys., 2010, **37**: 3541-3550. doi:10.1118/1.3427317

(47) **P. Andreo, A. E. Nahum**, *Stopping-power ratio for a photon spectrum as a weighted sum of the values for monoenergetic photon beams.* Physics in Medicine and Biology, 1985, **30**: 1055-1065.

(48) **H. Benmakhlouf, P. Andreo**, *Spectral distribution of particle fluence in small field detectors and its implication on small field dosimetry*. Med. Phys. 2017, **44**: 713-724.

(49) **J. Xue, J. D. McKay, J. Grimm, C.-W Cheng, R. Berg, S. –Y. L. Grimm, Q. Xu, G. Subedi, I. J. Das**, *Small field dose measurements using plastic scintillation detector in heterogeneous media*. Med. Phys. 2017, **44**: 3815-3820.

(50) **P. E. Galavis, L. Hu, S. Holmes, I. J. Das**, *Characterization of the plastic scintillation detector Exradin W2 for small field dosimetry*. Med. Phys. 2019, **46**: 2468-2476.

(51) **M. Yarahmadi, S. Wegener, O. A. Sauer**, *Energy and field size dependence of a silicon diode designed for small-field dosimetry*. Med. Phys., 2017, **44**: 1958-1964. doi:10.1002/mp.12195

(52) **J. Seuntjens**, *Small Field Radiation Therapy: Physics and Recent Recommendations from IAEA and ICRU*. Med. Phys. 2016, **43**: 3893-3893.

(53) **C. Weber, R. Kranzer, J. Weidner, K. Kröninger, B. Poppe, H. K. Looe, D. Poppinga**, *Small field output correction factors of the microSilicon detector and a deeper understanding of their origin by quantifying perturbation factors*. Med. Phys., 2020, doi:10.1002/mp.14149

(54) **I. J. Das, M. Kassaee, Alireza, Tochner, Zelig**, *Choice of Radiation Detector in Dosimetry of Stereotactic Radiosurgery-Radiotherapy*. Journal of Radiosurgery, 2000, **3**: 177-186.

(55) **H. Palmans, P. Andreo, M. S. Huq, J. Seuntjens, K. E. Christaki, A. Meghzifene**, *Dosimetry of small static fields used in external photon beam radiotherapy: Summary of TRS-483, the IAEA–AAPM international Code of Practice for reference and relative dose determination.* Med. Phys. 2018, 45

(56) **B. Casar, E. Gershkevitsh, I. Mendez, S. Jurković, M. S. Huq**, *A novel method for the determination of field output factors and output correction factors for small static fields for six diodes and a microdiamond detector in megavoltage photon beams*. Med. Phys. 2019, **46**: 944-963.

(57) **X. A. Li, M. Soubra, J. Szanto, L. H. Gerig**, *Lateral electron equilibrium and electron contamination in measurements of head-scatter factors using miniphantoms and brass caps.* Med. Phys. 1995, **22**: 1167-1170.

(58) **P. Papaconstadopoulos**. *On the detector response and the reconstruction of the source intensity distribution in small photon fields*. PhD thesis, McGill University, Montreal, 2016.

(59) **P. Andreo**. *REVIEW, The physics of small megavoltage photon beam dosimetry*. Radiotherapy and Oncology, 126 (2018), 205-213.

(60) **I. J. Das, G. X. Ding, A. Ahnesjö**, *Small fields: Nonequilibrium radiation dosimetry.* Med. Phys. 2008, **35**: 206-215.

(61) **J. W. Boag, J. Currant**, *Current collection and ionic recombination in small cylindrical ionization chambers exposed to pulsed radiation.* The British Journal of Radiology, 1980, **53**: 471-478.

(62) **F. DeBlois, C. Zankowski, E. B. Podgorsak**, *Saturation current and collection efficiency for ionization chambers in pulsed beams*. Med. Phys. 2000, **27**: 1146-1155.

(63) **M. F. Katumba**, MSc thesis, University of Witwatersrand/ school of physics, 2010.

(64) **O. A. Sauera, J. Wilbert**, Measurement of output factors for small photon beams, *Medical Physics*, 2007, **34**: 1983-1991.

(65) **IEC 60731**, *Medical electrical equipment-Dosimeters with ionization chambers as used in radiotherapy.* 2011.

(66) **PTW Freiburg**, *Detectors, Including Code of Practice*. 2018/2019

(67) **S. Wegener, A. O. Sauer**, *Energy response corrections for profile measurements using a combination of different detector types.* Med. Phys. 2018, **45**: 898-907

(68) **P. Andreo, A. Brahme**, *stopping power data for high-energy photon beams.* Phys. Med. Biol,, 1986, **31**: 839-858.

(69) **R. Alfonso, P. Andreo, R Capote, M. S. Huq, W. Kilby, et al.**, *A new formalism for reference dosimetry of small and nonstandard fields.* Med. Phys., 2008, **35**: 5179-5186

(70) **B. Casar, E. Gershkevitsh, I. Mendez, S. Jurković, M. S. Huq**, *Output correction factors for small static fields in megavoltage photon beams for seven ionization chambers in two orientations-perpendicular and parallel*. Med. Phys., 2020, **47**: 242-259.

(71) **S. Agostinelli, S. Garelli, M. Piergentili, F. Foppiano**, *Response to high-energy photons of PTW31014 PinPoint ion chamber with a central aluminium electrode*. Med. Phys., 2008, **35**: 3293-3301

(72) **C. Martens, C. De Wagter, W. De Neve**, *The value of the PinPoint ion chamber for characterization of small field segments used in intensity-modulated radiotherapy*, Phys. Med. Biol. 2000, **45**: 2519-2530

(73)

Appendix 1.

Manufacture Specification of PTW-31021 Semiflex 3D Ionization chamber

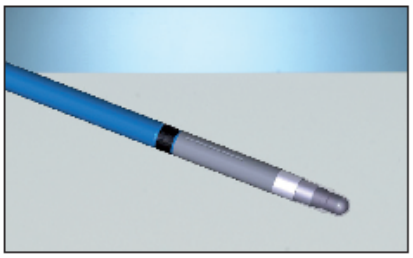

Semiflex 3D Chamber 0.07 cm³ Type 31021

Exceeds IEC 60731 and TG-51 requirements

Standard therapy chamber with excellent 3D characteristics for scanning systems and for absolute dosimetry

Highlights

- Waterproof, semiflexible design for easy mounting in scanning water phantoms
- Excellent 3D characterstics
- Sensitive volume of 0.07 cm³
- Outperforms all requirements of IEC 60731 and AAPM TG-51
- Designed for axial and radial irradiation

The 31021 Semiflex 3D chamber is ideal for dose measurements in small fields as encountered e.g. in IORT, IMRT and stereotactic beams as well as for dose measurements in standard fields up to 40 x 40 cm². Relative dose distribution can be measured with high spatial resolution in any direction. The waterproof, fully guarded chamber can be used in air, solid state phantoms and in water.

Specification

Type of product	vented cylindrical ionization chamber
Application	absolute dosimetry in radiotherapy beams
Measuring quantities	absorbed dose to water air kerma exposure
Reference radiation quality	^{60}Co
Nominal sensitive volume	0.07 cm³
Design	waterproof, vented, fully guarded
Reference point	on chamber axis, 3.45 mm from chamber tip
Direction of incidence	axial, radial
Nominal response	2 nC/Gy
Long-term stability	≤ 0.3 % over 2 years (*)
Chamber voltage	400 V nominal ± 500 V maximal
Polarity effect	photons ≤ ± 0.8 % electrons ≤ ± 1 %
Directional response	≤ ± 0.5 % for rotation around the chamber axis ≤ ±1 % for tilting of the axis up to ± 90°
Leakage current	≤ ± 4 fA
Cable leakage	≤ 100 fC/(Gy·cm)

Materials and measures

Wall of sensitive volume	0.57 mm PMMA, 1.19 g/cm³ 0.09 mm graphite, 1.85 g/cm³
Total wall area density	84 mg/cm²
Dimension of sensitive volume	radius 2.4 mm length 4.8 mm
Central electrode	Al 99.98, diameter 0.8 mm
Build-up cap	PMMA, thickness 3 mm

Ion collection efficiency at nominal voltage

Ion collection time	118 µs
Max. dose rate for ≥ 99.5 % saturation ≥ 99.0 % saturation	 6.7 Gy/s 13.4 Gy/s
Max. dose per pulse for ≥ 99.5 % saturation ≥ 99.0 % saturation	 0.68 mGy 1.42 mGy

Useful ranges

Chamber voltage	± (50 ... 400) V
Radiation quality	^{60}Co ... 50 MV photons (9 ... 45) MeV electrons
Field size	(2.5 x 2.5) cm² ... (40 x 40) cm² (3.0 x 3.0) cm² ... (40 x 40) cm² ≥ 18 MV
Temperature	(10 ... 40) °C (50 ... 104) °F
Humidity	(10 ... 80) %, max 20 g/m³
Air pressure	(700 ... 1060) hPa

Ordering Information

TN31021 Semiflex 3D chamber 0.07 cm³, connecting system BNT
TW31021 Semiflex 3D chamber 0.07 cm³, connecting system TNC
TM31021 Semiflex 3D chamber 0.07 cm³, connecting system M

Options

T48012 Radioactive check device ^{90}Sr
T48002.1.004 Chamber holder for check device

(*) expected value (chamber is not yet 2 years old)

D687.219.0201 Effective 2015-07
Previous specifications are void.

PTW-Freiburg · Lörracher Straße 7 · 79115 Freiburg, Germany
Phone: +49 761 49055-0 · Fax: +49 761 49055-70
info@ptw.de · www.ptw.de

PTW